Role of the supports during phosphorus poisoning of diesel oxidation catalysts

Chemical Engineering Journal 468 (2023) 143548

Contents lists available at ScienceDirect

Chemical Engineering Journal

journal homepage: www.elsevier.com/locate/cej

Role of the supports during phosphorus poisoning of diesel oxidation catalysts

Phuoc Hoang Ho *, Jieling Shao, Dawei Yao, Wei Di, Derek Creaser, Louise Olsson *

Chemical Engineering, Competence Centre for Catalysis, Chalmers University of Technology, SE-412 96 Gothenburg, Sweden

ARTICLE INFO

Keywords:
Diesel oxidation catalysts
Phosphorus poisoning
High siliceous zeolites
CO oxidation
NO oxidation
Hydrocarbon oxidation

ABSTRACT

Phosphorus (P) poisoning is one of the main factors accounting for the deactivation of diesel oxidation catalysts (DOC) apart from sulfur poisoning and sintering of the Pt active sites. This study compares the impact of P with loading up to 2.4 wt% on the catalytic performance of monometallic and bimetallic Pt-Pd catalysts using alumina and high silica BEA zeolites as the supports. P poisoning caused deactivation for CO, C_3H_6, C_3H_8 and NO oxidation; however, the degree of the impact of P in terms of temperatures at which 50% of the component is converted (T_{50}) depends not only on the types of the active phase (Pt and Pt-Pd) but also on the types of supports (alumina and BEA zeolite). The influence of P impregnation on the textural properties of the materials is more significant for zeolite than alumina-based catalysts, which is in line with the activity measurements. A weak interaction between P and high silica zeolite resulted in the formation of a prominent fraction of P_2O_5 in the P-Pt/BEA, whereas a strong binding between P and alumina accounted for a dominant fraction of phosphate in the P-Pt/Al_2O_3 as revealed by XPS and NMR measurements. Phosphorus compounds partially covered the available surface of the active sites and this lowered the catalytic activity. For alumina-based catalysts, P mainly reacted with the support and only deactivated a part of the active noble metals. Whereas, for zeolite-based catalysts, P existed mainly in the form of phosphorus oxides that significantly blocked the catalyst surface and thereby deactivated more of the available active sites than that on alumina-based materials, which is consistent with the CO chemisorption data.

1. Introduction

Diesel oxidation catalyst (DOC) is typically the front unit of the Exhaust gas After-Treatment System (EATS) integrated with sequential units, namely, DOC, diesel particulate filter (DPF), selective catalytic reduction of NO_x with NH_3 (NH_3-SCR), and ammonia slip catalyst (ASC) for the treatment of the exhaust gas from vehicles using diesel engines [1]. The EATS plays a key role to meet the implementation of increasingly strict emission standards. The main contributions of DOC in the EATS are to oxidize CO and hydrocarbons to nontoxic products such as CO_2 and H_2O. The DOCs also convert NO by either reducing with HCs to N_2 and N_2O or oxidizing it with O_2 to NO_2. Although NO_2 is still a harmful gas, it is known to facilitate the conversion of total NO_x ($NO + NO_2$) by the reduction of NH_3 via a fast SCR reaction. Therefore, a mixture of NO and NO_2 with $NO_2/NO_x = 0.5$ is preferred for the input of the NH_3-SCR unit [2,3].

Over five decades, the development of DOC has been extensively established [4]. Platinum group metals (PGM) are inevitably used due to their exceptional activity under harsh operating conditions of diesel exhaust gases, e.g. large amounts of H_2O, multiple pollutants, an extremely lean mixture, and the presence of poisoning agents [4]. Bimetallic Pt-Pd active phases supported on alumina-based supports are typical formulations and they are deposited on cordierite honeycomb monoliths via a washcoating process. The Pt-Pd alloys have better resistance to sintering than their monometallic counterparts [5]. The ratio of Pt/Pd can be tailored to improve catalytic performance. However, to meet the more stringent legislation with very low limits for pollutants in the exhaust gas, it is necessary to understand and predict the stability of the DOC during the lifetime of the vehicle. Deactivation of the DOC is related to the operation at high temperatures and exposure to poisoning agents. High-temperature operation induces the sintering of noble metals while poisoning causes chemical reactions with the support and active sites, resulting in a pore blockage and surface area decrease. Sulfur (S) and phosphorus (P) are the two main poisoning elements for DOC. The former originates mainly from organic sulfur compounds in diesel fuels, for example, approximately 5 – 10 ppm in

* Corresponding authors.
E-mail addresses: phuoc@chalmers.se (P.H. Ho), louise.olsson@chalmers.se (L. Olsson).

https://doi.org/10.1016/j.cej.2023.143548
Received 26 January 2023; Received in revised form 18 April 2023; Accepted 13 May 2023
Available online 15 May 2023

ultra-low sulfur diesel (ULSD) [6], while the latter comes from the additive of engine lubricants, e.g. zinc dialkyl dithiophosphate (ZDDP) [4,7]. Sulfur in the form of SO_2 from the exhaust gas can be further oxidized to SO_3 under lean conditions and SO_x (i.e. SO_2 and SO_3) are poisoning agents for the DOC. SO_x deactivate PdO sites by directly reacting to form $PdSO_4$ whereas they block Pt sites by decreasing the oxygen adsorption at high temperatures [7]. Noticeably, SO_3 is highly corrosive by forming sulfuric acid. The impact of sulfur poisoning on the activity of DOC has been thoroughly summarized by Yang et al. in a recent review [8]. Regarding phosphorus poisoning, ZDDP can be dissociated into molecular fragments or transformed into phosphoric acid and these ZDDP-derived phosphorus compounds are emitted in the exhaust gas [9].

Phosphorus poisoning for DOC has gained attention in some recent publications [10–15] although a few pioneering works were previously published [16]. These studies focused on the characterization of the DOC (both model and real substrates from engines) and tests at the laboratory scale to elucidate the impact of P poisoning on oxidation activity. Notably, all the catalysts in these works are based on alumina or mixed oxides as the supports of the catalysts. It was found that P accumulation was unevenly distributed through the DOC unit in which the P content was higher for the surface than the bulk layer and it decreased from the inlet to the outlet [12,13,16]. At the laboratory scale, P can be introduced by either a direct injection of a phosphoric acid solution into the gas flow or pre-impregnation on the powder catalysts/honeycomb monolith with a P-containing precursor [13]. The direct introduction of phosphorus precursors imitates more the case in the real world. However, it is complicated to compare catalysts with supports that have a different affinity for P interaction using the direct injection method, since they will accumulate different amounts of phosphorus on them when exposing the catalysts to the same duration and concentration of P-solution. In contrast, the introduction of P by a pre-impregnation method generates a better homogeneity of P distribution and the exact amount of P can easily be steered, subsequently providing more information on the properties of the catalyst, especially the interaction of P with the catalysts.

In an early study using real catalysts from taxicabs (102,000 – 120,000 miles), Rokosz et al. found that phosphorus contamination was present in both the overlayer and within washcoat layer via the formation of Zn-, Ca-, Mg-, Al- and Ce(III)- phosphate and this caused a loss of specific surface area and consequently resulted in a strong deactivating effect, e.g. for C_3H_6 oxidation due to diffusion limitations [16]. This has been later confirmed in some studies, and the deactivation was observed not only for hydrocarbons but also for CO and NO oxidation; however, the impact was more pronounced for NO oxidation [12,13]. Regarding the interaction of P with the active sites, Anguita and coworkers have observed that the formation of phosphate blocked the active Pt sites and subsequently severely inhibited NO oxidation on Pt-Pd /$CeZrO_2$/La-Al_2O_3 catalyst [10]. P poisoning did not significantly induce the sintering of noble metal particles on alumina-based supports, but it did alter the morphology of the Pt particles, especially under a lean exhaust environment [17–21]. The impact of P poisoning on a DOC using zeolites has been rarely reported in the literature, although this topic is well documented for the selective catalytic reduction (SCR) of NO_x [22]. In the field of SCR of NO_x in which small pore zeolites are preferably used, P can block the pores of the zeolite supports and interact with the active elements (e.g. Cu and Fe), causing changes in both specific surface area and redox properties of the catalysts [22]. For a DOC, Kröger and coworkers found that P poisoning caused an increase in the Pt particle size of a Pt/ZSM-5 catalyst with a low silica content ($SiO_2/Al_2O_3 = 39$).

Diesel oxidation catalysts, based on zeolite supports containing high silica contents have been reported to have higher activity than their counterparts with low silica amounts. However, to the best of our knowledge, there are no studies available on the impact of P poisoning on DOC using high silica-alumina ratio (SAR) supports, which is the objective of the current paper. This paper focuses on the effect of P poisoning on the physicochemical properties and oxidation activity of the DOC using beta zeolite with high SAR in comparison with their counterparts using alumina as the support. Two series of monometallic (Pt) and bimetallic (Pt-Pd) catalysts with different P contents were prepared. The catalysts, both fresh and P-poisoned, are characterized with several characterization techniques including X-ray diffraction (XRD), inductively coupled plasma sector field mass spectrometry (ICP-SFMS), high-resolution transmission electron microscopy (HRTEM), scanning electron microscopy (SEM), N_2 physisorption, X-ray photoelectron spectroscopy (XPS), solid-state nuclear magnetic resonance (NMR), temperature-programmed desorption of NO (NO-TPD), and CO adsorption to correlate the physicochemical properties and the oxidation activity of the catalysts.

2. Experimental

2.1. Catalyst preparation

Beta zeolite (CP811C300, H^+ form) and ɣ-alumina (SBa-200) were purchased from Zeolyst and Sasol, respectively, and then calcined at 550 °C for 6 h before being used as supports for the preparation of the catalysts. The beta zeolite has a high Si content with SiO_2/Al_2O_3 of 217 (from elemental analysis) as this type of support showed advantages in the oxidation activity compared to the zeolite with low Si content [23]. Monometallic catalysts containing 2 wt% Pt were prepared with an incipient impregnation method and calcined at 550 °C for 2 h as described in our previous study [24] and denoted as Pt/Al_2O_3 and Pt/BEA for alumina and beta zeolite supports, respectively. These parent catalysts were pretreated with a degreening protocol (see section 2.4.1 in reference [25]) so that the catalysts would be stable to mimic the state of the catalysts in the catalytic converter before being poisoned with P. After pretreatment, the catalysts are denoted as degreened samples. The degreened catalysts were then impregnated with $(NH_4)_2HPO_4$ to achieve a target loading of 0.4 and 0.8 mmol P per gram of catalyst (0.4 and 0.8 mmol g^{-1}). The samples were subsequently calcined at 500 °C for 2 h to stabilize the interaction between P and the catalysts. We note that the loading of 0.8 mmol g^{-1} is equal to 2.4 wt% P which is a common value to study the effect of P poisoning reported in the literature [13]. The catalysts containing P were denoted as xP-Pt/A where × indicates the P loading (0.4 and 0.8 mmol g^{-1}) and A is the support (Al_2O_3 and BEA). It should be noted that the impregnation of phosphorus precursor into the catalysts was selected to have a homogeneous distribution of P species as well as a precise dosing of P species on catalysts with different affinities to phosphorus. With this method we can study the chemistry of P poisoning, for example, to differentiate the characteristics of the interactions between P species and two types of DOC based on alumina and high-silica beta zeolite. However, in the real case, phosphorus compounds deposit inhomogeneously on the washcoat and generally its content decreases both axially and radially, more near the inlet than the outlet of the DOC unit [4,12,13].

The bimetallic catalysts with Pt and Pd had a molar ratio Pt/Pd = 3/1 (corresponding to a mass ratio of 5.8/1) and contained the same total moles of noble metals as that of monometallic the Pt catalyst (2 wt% Pt). This corresponds to approximately 1.5 wt% Pt and 0.26 wt% Pd. These catalysts were prepared with a sequential impregnation of Pd and Pt as described elsewhere [26]. The bimetallic catalysts were poisoned with a P loading of 0.8 mmol g^{-1} using the same protocol as previously used for the monometallic Pt catalysts. These catalysts were denoted as 0.8P-Pt3Pd1/Al_2O_3 and 0.8P-Pt3Pd1/BEA.

The powder of each catalyst (without and with P) was deposited on honeycomb monoliths (cordierite, Ø = 21 mm, L = 20 mm, 188 channels) with a solid loading of 500 ± 10 mg using a standard washcoating method with 5 wt% boehmite as a binder [25].

2.2. Characterizations

The Si/Al ratio of the beta zeolite and loadings of Pt, Pd, and P were determined using inductively coupled plasma sector field mass spectrometry (ICP-SFMS) performed at ALS Scandinavia (Luleå, Sweden). N_2 physisorption at −196 °C was performed using a Micromeritics Tristar instrument. X-ray diffraction (XRD) was performed using a D8 Advance Diffractometer (Bruker AXS, Germany, CuK_α radiation). X-ray photoelectron spectroscopy (XPS) was performed with a Perkin-Elmer PHI 5000 VersaProbe III – Scanning XPS Mircoprobe^{TM} apparatus. HRTEM (High-resolution transmission electron microscopy) images were recorded with an FEI Titan 80–300 microscope (Cs-corrector probe, energy dispersive spectroscopy (EDS) and high-angle annular dark-field (HAADF) detector). Scanning electron microscopy (JOEL 7800F Prime instrument) was used to acquire elemental maps. Detailed information on the methods and the instruments can be found elsewhere [25].

Solid-state nuclear magnetic resonance (NMR) measurements were performed on a Bruker Advance III 500MHZ magnet spectrometer equipped with a 4 mm double-resonance magic angle spinning (MAS) probe. All chemical shifts were referred to as the standard chemical shift at 34.48 ppm of the methylene (–CH_2-) group of adamantane ($C_{10}H_{16}$).

Temperature-programmed desorption of NO (NO-TPD) was measured using a calorimeter (Setaram Sensys). Approximately 30 mg of sample (180–250 μm) was loaded into a fixed-bed reactor (quartz, inner diameter of 4 mm) and then treated in Ar at 300 °C for 30 min. The adsorption of NO was performed at 30 °C by introducing a flow containing 2000 ppm of NO in Ar through the sample for 1.5 h. The weakly-adsorbed NO was then removed by flushing the sample with Ar for 1 h. After that, the reactor was heated up from 30 to 700 °C with a heating rate of 10 °C min^{-1}. The desorption of NO was monitored by tracking the mass number of $m/z = 30$ using a mass spectrometer (HPR-20 QIC).

CO adsorption was performed using an ASAP2020 Plus from Micromeritics. The powder sample (approximately 0.12 g) was reduced in hydrogen at 400 °C for 1 h and then evacuated to 5 μmHg at 35 °C. The adsorption isotherms of CO at 35 °C were measured from 100 to 600 mmHg with intervals of 25 mmHg. The amount of CO adsorption was calculated from the intercept using a linear fitting curve of the isotherm.

2.3. Catalytic tests

The degreening step of the powder catalysts prior to impregnating with P as well as the activity tests were performed in a flow reactor system equipped with one horizontal quartz tube (D × L = 2.1 cm × 78 cm) and a heating system controlled via a Eurotherm controller. The gas flow was steered using Bronkhorst® mass flow controllers (MFC) and the water using a Bronkhorst® CEM system. The gases were analysed using a MultiGasTM 2030 FTIR from MKS.

2.3.1. Degreening of the powder catalyst

Before doing the impregnation with $(NH_4)_2HPO_4$, the powder catalysts were pretreated with a degreening protocol to stabilize the active phase of the catalysts. The powder sample was distributed in an alumina crucible which was then placed in the reactor tube. The sample was firstly treated in 2 vol% H_2 and 5 vol% H_2O/Ar at 500 °C for 30 min and subsequently oxidized in a mixture of 500 ppm NO, 8 vol% O_2, and H_2O/Ar at 700 °C for 2 h. After that, the reactor was cooled to 500 °C under the same gas mixture. The sample was treated in five sequential steps, where each step was 15 min for each. The gas compositions were (i) 10 vol% O_2 and 5 vol% H_2O/Ar, (ii) 5 vol% H_2O/Ar, (iii) 1 vol% H_2 and 5 vol% H_2O/Ar, (iv) 5 vol% H_2O/Ar and (v) 10 vol% O_2 and 5 vol% H_2O/Ar. Then the reactor was cooled to 120 °C in 10 vol% O_2 and 5 vol% H_2O/Ar and then from 120 °C to room temperature in Ar. This five-step procedure, denoted pretreatment, was employed. This protocol was chosen since platinum and palladium are present in these catalysts and the oxidation state of the noble metals will influence the activity of the catalysts. We therefore first reduced the catalysts and then had a fixed time for oxidation, in order to make the oxidation as controlled as possible. In between these steps, flushing was conducted.

2.3.2. Activity test

The activity test was performed with one coated monolith. Prior to each ramping experiment, the catalyst was pretreated in five steps, each 15 min and with the same gas concentrations as for the five steps in the degreening (Section 2.3.1). Then the catalyst was cooled to 120 °C. After that, a gas mixture containing 1000 ppm CO, 500 ppm C_3H_6, 500 ppm C_3H_8, 500 ppm NO, 10 vol% O_2, and 5 vol% H_2O was fed into the reactor. After 45 min when the concentration of all gas components had been stable, the temperature was ramped up from 120 to 500 °C with a heating rate of 5 °C min^{-1}. The reactor was held at 500 °C for 30 min and then cooled down to 120 °C in the same gas mixture. Five cycles were repeated for each catalyst.

3. Results and discussion

3.1. Characterization of catalysts

The Pt, Pd, and P contents of all catalysts measured by ICP-SFMS are shown in Table 1. Pt loadings of monometallic catalysts were in a range from 1.61 to 1.74 wt%. Both Pt/Pd ratio and P loadings were similar to the theoretical values. For example, the Pt3Pd1/Al_2O_3 and Pt3Pd1/BEA catalysts exhibited a molar ratio of Pt/Pd around 3.1 (mass ratio of 5.8 in Table 1) while P loadings were around 1.2 and 2.4 wt% for the samples loaded with 0.4 and 0.8 mmol g^{-1}, respectively.

During the calcination, the $(NH_4)_2HPO_4$ precursor was decomposed into different species from various reactions as follows [27,28]:

$$(NH_4)_2HPO_4 \rightarrow NH_4H_2PO_4 + NH_3\uparrow \quad (1)$$

$$NH_4H_2PO_4 \rightarrow H_3PO_4 \text{ (phosphoric acid)} + NH_3\uparrow \quad (2)$$

$$2H_3PO_4 \rightarrow H_4P_2O_7 \text{ (pyrophosphoric acid)} + H_2O\uparrow \quad (3)$$

$$2H_4P_2O_7 \rightarrow P_4O_{10} + 4H_2O\uparrow \quad (4)$$

The phosphorus oxide (P_4O_{10} or empirical formulation of P_2O_5) can physically deposit on the support of the catalysts (alumina and zeolite) while phosphoric acid and pyrophosphoric acid can chemically react with the supports (alumina or zeolite) to form, for example, aluminum phosphate ($AlPO_4$) and pyrophosphate $Al_4(P_2O_7)_3$. These interactions subsequently modified the physicochemical properties of the catalysts [22].

Nitrogen physisorption data revealed a decrease in total pore volume and subsequently specific surface area (S_{BET}) with an increase in phosphorus loadings. This trend was similar to that reported by Kröger and coworkers for a Pt/Al_2O_3 catalyst [19]. Notably, the decremented level of the specific surface area is proportional to the phosphorus content (Fig. S1), agreeing well with the literature [29]. The specific surface area decreased by approximately 12% and 30% with a loading of 0.8 mmol g^{-1} on Pt/Al_2O_3 and Pt/BEA, respectively. This indicates that the impact of P on the textural properties was more pronounced on Pt/BEA than on Pt/Al_2O_3. Both parent bimetallic catalysts Pt3Pd1/Al_2O_3 and Pt3Pd1/BEA had very similar S_{BET} and total pore volume as their monometallic Pt counterparts. Loading P with 0.8 mmol g^{-1} on these bimetallic catalysts resulted in a loss of approximately 15% and 32% of S_{BET} for Pt3Pd1/Al_2O_3 and Pt3Pd1/BEA, respectively. The trend in the loss of S_{BET} on bimetallic catalysts after being loaded with P is almost the same as that on monometallic catalysts. In both cases, a more significant loss of specific surface area was found on the zeolite-based catalysts impregnated with P than on the alumina counterparts. A larger number of pores in the zeolites were blocked by phosphorus species compared to those of alumina due to the smaller pores of the zeolite than alumina (Fig. S2). In the literature, a severe decrease in micropore volume and

Table 1
Physicochemical properties of the catalysts.

Catalyst	Pt[a] / wt.%	Pd[a] / wt.%	Pt/Pd molar ratio	P[a] / wt.%	S_{BET} / m^2 g^{-1}	V_{pore} / cm^3 g^{-1}	CO uptake[b] / cm^3 g^{-1} (STP)	NO uptake[c] / μmol g^{-1}
Pt/Al_2O_3	–	–	–	–	169	0.48	0.25	11.9
0.4P-Pt/Al_2O_3	1.74	–	–	1.24	158	0.46	0.18	14.4
0.8P-Pt/Al_2O_3	1.66	–	–	2.40	148	0.43	0.16	15.8
$Pt3Pd1/Al_2O_3$	–	–	–	–	171	0.48	–	11.6
0.8P-$Pt3Pd1/Al_2O_3$	1.33	0.23	3.14	2.30	146	0.43	–	15.5
Pt/BEA	–	–	–	–	609	0.34	0.23	8.9
0.4P-Pt/BEA	1.65	–	–	1.16	513	0.29	0.09	7.6
0.8P-Pt/BEA	1.61	–	–	2.28	424	0.26	0.07	7.2
Pt3Pd1/BEA	–	–	–	–	609	0.34	–	7.0
0.8P-Pt3Pd1/BEA	1.30	0.23	3.07	2.30	414	0.25	–	7.3

[a] Determined with ICP-SFMS [b] From CO adsorption [c] From NO-TPD.

specific surface area due to the phosphatization of zeolites has been widely reported [22].

Fig. 1 presents the XRD patterns of different catalysts before and after being loaded with P. It should be noted that the reflections of the beta zeolite in the Pt3Pd1/BEA sample exhibited higher intensity compared to Pt/BEA, and the reason for this could be that the Pt3Pd1/BEA was calcined one more time when adding the two noble metals by a sequential impregnation. It was observed that a clear decrease in the intensity for the reflection around 2θ of 22.5° for the 0.8P-Pt/BEA and 0.8P-Pt3Pd1/BEA compared to the Pt/BEA. This indicates crystallinity

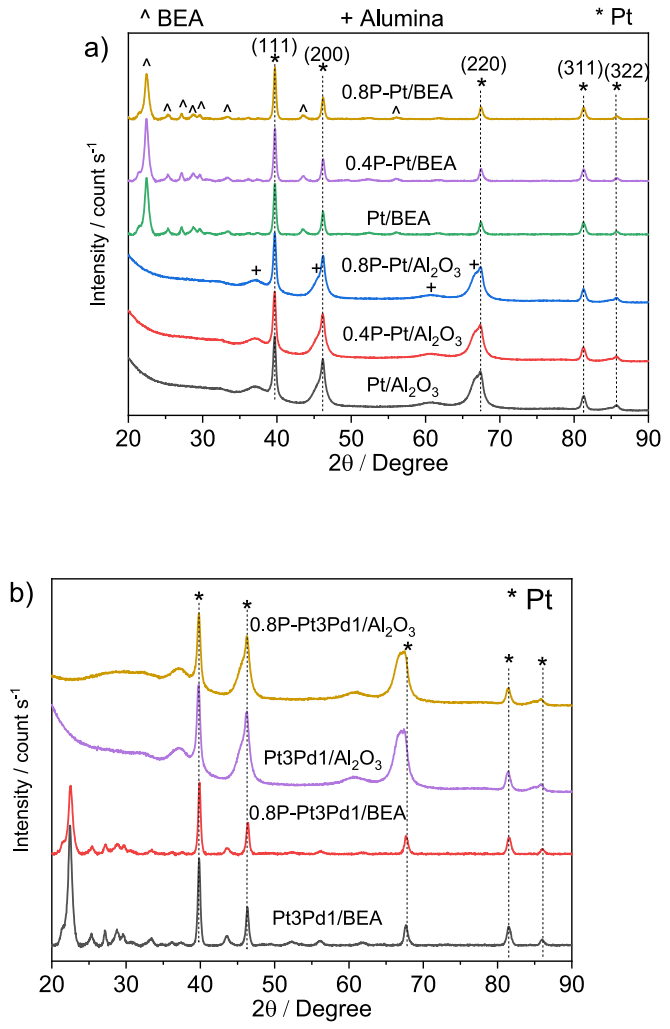

Fig. 1. XRD patterns of parent and P-containing catalysts: a) monometallic and b) bimetallic catalysts.

loss of zeolite beta to some extent due to either the partial extraction of aluminum from the framework of the zeolite (dealumination) by phosphoric acid to form $AlPO_4$ [22] or the effect temperature during the calcination after the impregnation of $(NH_4)_2HPO_4$ precursor. It should be noted that the beta zeolite used in the present work has very low alumina content (molar ratio of SiO_2/Al_2O_3 around 217, silica-rich). Therefore, it is expected that only a small amount of $AlPO_4$ can be formed. The loss of the intensity of alumina reflection was not significant for alumina-based catalysts (Fig. S3). It is known that during calcination, phosphoric acid may react with Al_2O_3 to form aluminum phosphate [30]. There are different results found in the literature regarding P-containing phases, which shows that it is a very complicated process. For alumina-based catalysts, some studies observed the formation of $AlPO_4$ by the presence of a reflection at 2θ of around 22.5° [31,32]. For zeolite-based materials, many studies have reported no diffractions of new phases related to P-containing compounds even with higher P loadings [29,33–35]. In our work, no new diffractions related to $AlPO_4$ were observed in the P-modified samples; however, their presence was confirmed later by XPS and NMR (Figs. 3–5). Therefore, $AlPO_4$ was probably formed in an amorphous phase, or very small amounts, or with a small crystallite size below the detection limit of XRD. This agrees with the data reported by Wang et al. for the impregnation of 2.7–7.1 wt% of P in a mixture of zeolite and alumina binder [34]. Apart from the reflections of the zeolite or alumina support, other diffractions were assigned to metallic Pt (ICDD2020, PDF #01-070-2057). We also observed the formation of Pt-Pd alloy with shifting of Pt reflection to a higher diffraction angle in the cases of the bimetallic Pt-Pd samples than monometallic ones (Fig. S4), as reported in the literature [25,26,36]. However, there was no significant difference in the Pt reflections between the parent and the P-modified samples.

Fig. 2 displays representative STEM images (HAADF mode) of Pt particles taken from different parent and P-poisoned catalysts. The Pt/Al_2O_3 catalyst had a bimodal distribution, with both small and large particles with an average size of approximately 2 nm (120 particles) and 20 nm (126 particles) (Fig. 2a), respectively, which was similar to our previous work [24]. An example of one location having some small particles is shown in Fig. S5. In the 0.8P-Pt/Al_2O_3 sample, only large particles were observed with an average size of around 24 nm (Fig. 2b). It should be noted that the different conditions of treatment between Pt/Al_2O_3 and 0.8P-Pt/Al_2O_3 were only the calcination step after the impregnation of $(NH_4)_2HPO_4$. The small particles observed in the Pt/Al_2O_3 (after the degreening) could have further sintered during the calcination step at 500 °C in the presence of P and therefore they disappeared in the 0.8P-Pt/Al_2O_3. However, it is not clear if the addition of P could induce the sintering since TEM is only examining a very small part of the surface. For the case of zeolite samples, average particle sizes of approximately 16 nm were observed for both Pt/BEA and 0.8P-Pt/BEA samples. This suggests that the presence of P had no significant effect on the sintering of Pt species in the 0.8P-Pt/BEA catalyst. Furthermore, both phosphorus-containing bimetallic catalysts (0.8P-

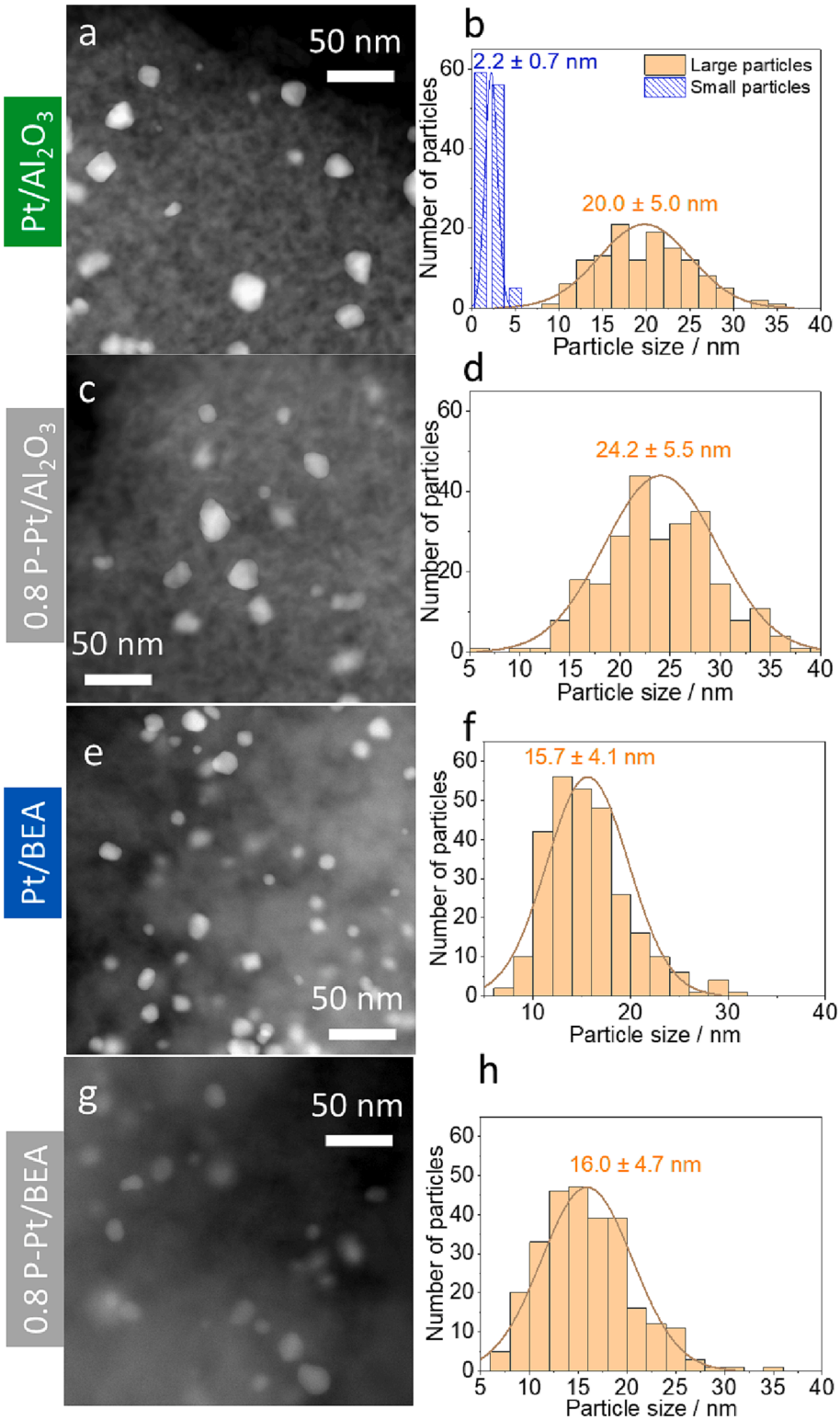

Fig. 2. TEM images (a, c, e, g) and particle distributions (b, d, f, h) of monometallic catalysts without and with P. Note that Pt/Al_2O_3 and Pt/BEA were treated at 700 °C for 2 h in a mixture of 500 ppm NO + 10 vol% O_2 + 5 vol% H_2O before impregnation with P. The P-containing samples were then calcined at 500 °C for 2 h.

$Pt3Pd1/Al_2O_3$ and 0.8P-Pt3Pd1/BEA) showed a similar average particle size of approximately 15 nm (Fig. S6) which was similar to the average sizes of Pt in their monometallic counterparts.

The elemental distributions of phosphorus-containing bimetallic catalysts from TEM measurements are shown in Fig. S7. We attempted to verify a relative distribution of P toward the noble metals (Pt and Pd) or the supports (alumina and zeolite). Unfortunately, the X-ray energy of P-Kα (2.013 KeV) overlaps with Pt-M (2.048 KeV) making it difficult to distinguish the maps between them [37]. Furthermore, a clear overlap between Pt and Pd distribution on large particles indicated the formation of Pt-Pd alloys, which agrees well with the XRD data as reported in our previous work [26]. In literature, SEM is usually used to measure the

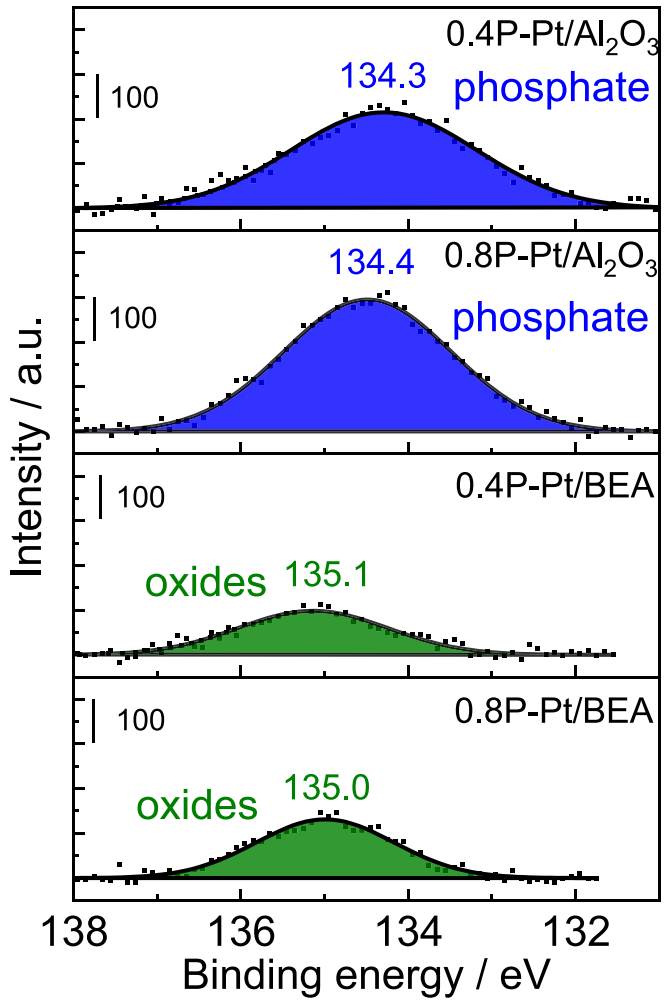

Fig. 3. XPS measurements of different monometallic catalysts. Note deconvolution was not performed.

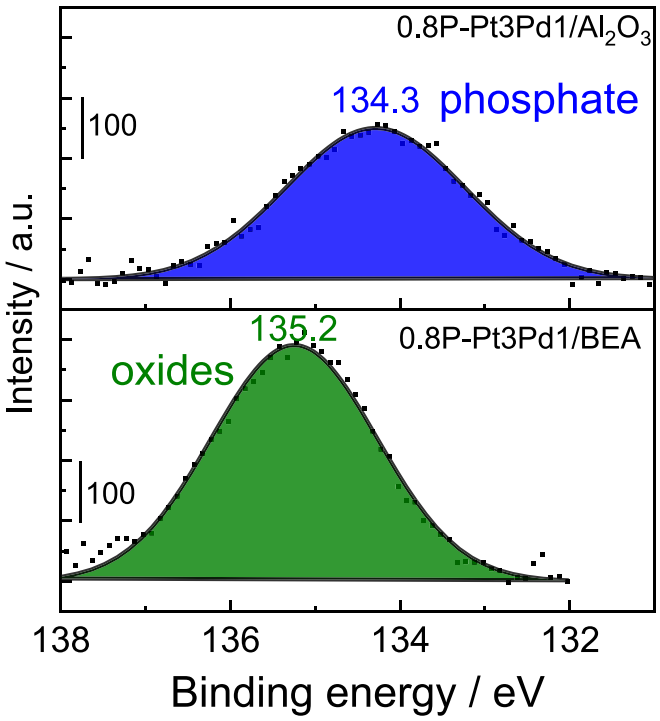

Fig. 4. XPS measurements of different bimetallic catalysts. Note deconvolution was not performed.

distribution of phosphorus elements [13,21]. Elemental distributions of 0.8P-Pt/BEA and Pt/BEA are shown in Figs. S8 and S9, respectively. For the 0.8P-Pt/BEA, the maps of P and Pt overlapped with those of Si, Al, and O, indicating a homogenous distribution of these elements in the sample. However, as mentioned previously that the overlapping of the energy between Pt and P elements caused a big issue for the interpretation of their mapping due to interference. To prove this, we predefined the element P before the acquisition of analysis of the Pt/BEA catalyst (without the impregnation of P). As shown in Fig. S9, the map of the P element was similar to the map of Pt, even though this sample did not contain P. Therefore, the interpretation of SEM mapping of P and Pt needs to be performed with caution.

XPS measurements provide information on the chemical state of P and Pt (Pd) in both monometallic and bimetallic catalysts and subsequently allow interpretation of how P interacts with the support (alumina, zeolite) and the noble metals (Pt, Pd) of the catalysts. Binding energies of P 2p, Pt 4f7/2, and Pd 3d5/2 core levels are summarized in Table 2, while the XPS spectra and the detailed information of the deconvolution are plotted in Figs. 3, 4, S10, and S11. Starting with P 2p core levels for monometallic catalysts (Fig. 3), the spectra of P 2p for 0.4P-Pt/Al_2O_3 showed broad peaks centered at approximately 134.3 eV, which possibly attributed to $AlPO_4$ [38]. Whereas that for 0.4P-Pt/BEA had a peak at higher BE, around 135.1 eV, which was assigned to phosphorus pentoxide [39,40]. A significant difference in the binding energies indicated different phosphorus species were present on the surface of the two catalysts. Increasing P loading from 0.4 to 0.8 mmol g^{-1}, resulted in an increase in the intensity of the peak due to more P on the surface but the peak position was almost unchanged. For the bimetallic samples, a similar trend was found, namely, phosphate was the main specie of the P surface compound in the alumina-based catalyst (0.8P-Pt3Pd1/Al_2O_3) whereas P_2O_5 was predominant in the zeolite-based catalyst (0.8P-Pt3Pd1/BEA) (Fig. 4). It should be noted that the assignment of the binding energy of the P 2p core level to different phosphorus species is quite complicated [41]. To avoid any biased interpretation of the deconvolution of the peak, it was only discussed from the original data and no deconvolution was performed. We assigned the dominating peak, thus, it is possible that some phosphates are present in the zeolite samples, as well as some phosphorus pentoxide can be present in alumina samples. More detailed information on the phosphorus species will be investigated by the solid-state NMR in the next section.

The binding energy of Pt increased slightly from 71.5 eV in Pt/Al_2O_3 to 71.8 eV in 0.8P-Pt/Al_2O_3 but was almost unchanged between Pt/BEA and 0.8P-Pt/BEA (Table 2). The slight increase in the binding energy of Pt 4f7/2 in the sample 0.8P-Pt/Al_2O_3 (~0.3 eV) indicated mild oxidation of Pt which could be related to the oxidation of small Pt particles during the secondary calcination after the impregnation of the precursor of P. This is in line with the observed changes in Pt particle size in the TEM images. It should be noted that the overlapping binding energy between Pt 4f7/2 and Al 2p as well as a low loading of Pt make it difficult to deconvolute the peaks for Pt/Al_2O_3 into different oxidation states of Pt species for alumina-based catalysts (Fig. S10a). For Pt/BEA, the peak of Pt 4f7/2 was deconvoluted and the percentage of Pt^{+2} and Pt^0 was approximately 29% and 71%, respectively. The presence of P did not alter the ratio of Pt^{+2} and Pt^0 (Table 2). In the literature, smaller Pt particles were reported to be oxidized easier than the larger particles and this usually resulted in a change in Pt^0/Pt^{+2} ratio. Therefore, no change in Pt^0/Pt^{+2} ratio suggests that the presence of P did not induce the sintering of Pt particles in the Pt/BEA catalysts, which is in line with the TEM data. For the bimetallic samples without P (Pt3Pd1/Al_2O_3 and Pt3Pd1/BEA), the metallic phases of Pt and Pd were identified by Pt 4f7/2 around 71.2 eV and Pd 3d5/2 around 335.5 eV, respectively (Table 2

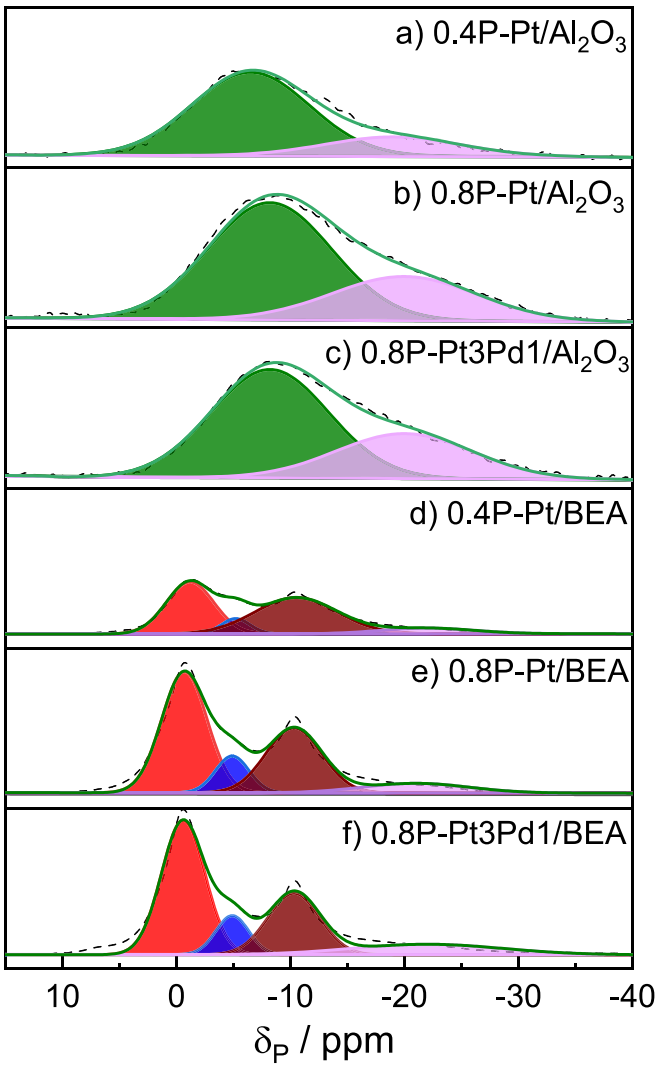

Fig. 5. ^{31}P MAS NMR spectra of parent and phosphorus-impregnated catalysts.

Table 2
Binding energy BE (eV) of P 2p, Pd 3d5/2, and Pt 4f7/2 for different catalysts.

Catalyst	P *2p*	Pt *4f7/2*	Pt^{+2} / %	Pt^{0} / %	Pd *3d5/2*
Pt/Al_2O_3	–	71.5	n.d.	n.d.	–
$0.4P\text{-}Pt/Al_2O_3$	134.4	71.6	n.d.	n.d.	–
$0.8P\text{-}Pt/Al_2O_3$	134.4	71.8	n.d.	n.d.	–
$Pt3Pd1/Al_2O_3$	–	71.2	n.d.	n.d.	335.4
$0.8P\text{-}Pt3Pd1/Al_2O_3$	134.3	71.4	n.d.	n.d.	336.2
Pt/BEA	–	71.5	29	71	–
0.4P-Pt/BEA	135.0	71.4	29	71	–
0.8P-Pt/BEA	135.0	71.4	26	74	–
Pt3Pd1/BEA	–	71.1	n.d.	n.d.	335.6
0.8P-Pt3Pd1/BEA	135.2	71.6	n.d.	n.d.	335.8

and Fig. S11). In the presence of P, these metallic phases were partially oxidized as indicated by a slight shift of BE to a higher value for both Pt and Pd (Table 2). For example, the BE of Pt 4f7/2 on 0.8P-Pt3Pd1/BEA was shifted 0.5 eV higher than that on Pt3Pd1/BEA while the BE of Pd 3d5/2 on $0.8P\text{-}Pt3Pd1/Al_2O_3$ was shifted to 0.8 eV higher than that for $Pt3Pd1/Al_2O_3$ (Table 2). It should be noted that the data of ex situ XPS only provide a relative comparison of the oxidation states of Pt and Pd of the catalysts before and after phosphorus impregnation. However, these oxidation states can be drastically changed in the presence of different gases (CO, O_2, NO, hydrocarbon, and H_2O) under the reaction conditions. Therefore, it is difficult to make a direct correlation between the oxidation states of Pt and Pd and the performance of the catalysts.

The structure of phosphorus-containing species, when P interacts with the alumina and zeolite supports, was probed by solid-state ^{31}P NMR. In general, an interaction between phosphate precursor and oxide support is specified by how terminal O in the PO_4 tetrahedron coordinates with the oxides of the supports and noted as Q^n in which n (n = 0, 1, 2, and 3) is the number of P-O-P linkages of an individual phosphate tetrahedron [42]. Pure solid phosphate contains only a network of Q^3 groups. When the phosphate species are dispersed on alumina or zeolite, some of the oxygen atoms can interact with Al via a P-O-Al coordination, and these oxygen atoms are denoted terminal O. Fig. 5 shows the ^{31}P resonances of alumina-based and zeolite-based catalysts with two different loadings of P. The ^{31}P spectra of alumina-based catalysts show asymmetric peaks with a tail at low frequencies. The peaks for $0.8P\text{-}Pt/Al_2O_3$ and $0.8P\text{-}Pt3Pd1/Al_2O_3$ were more intense than that for $0.4P\text{-}Pt/Al_2O_3$. These peaks were deconvoluted into two peaks at around – 8 and −20 ppm chemical shifts, which were assigned to P in pyrophosphate or P-O-Al terminal groups (monophosphate) and P-O-P linkages in polyphosphates (or $AlPO_4$), respectively [30,42,43]. We note that in the literature, the chemical shift at around 0 ppm was assigned to free monomeric orthophosphate (P_2O_5/P_4O_{10}) [44]. The small contribution of this chemical shift into the first peak of the spectra could not be excluded since there was a small overlap. However, the fitting of the curve suggests that there is no or only a minor peak around 0 ppm; therefore, we only considered the contribution of two peaks at −8 and −20 ppm in the fitting of the data for the alumina-based samples.

To measure the sites where Al and P atoms are linked in more detail, ^{27}Al solid-state MAS-NMR spectra were collected for all catalysts and displayed in Fig. 6. The spectrum of Pt/Al_2O_3 (without P) showed two peaks centered at 10.1 and 67.2 ppm chemical shifts, which were characteristic of Al^{3+} ions in octahedral and tetrahedral coordination, respectively [45]. The intensity of the peak centered at 10.1 ppm in the spectra of the P-containing materials decreased with an increase in P loading and the relationship is linear (Fig. 6c). Notably, the intensity of the peak at 67.2 ppm was not changed. This indicates that P tended to interact with Al^{3+} octahedral sites but not the tetrahedral sites and subsequently resulted in a drop in the number of these Al^{3+} octahedral sites.

The ^{31}P spectra of the zeolite-based catalysts showed two major resonances at approximately 0 and −11 ppm and two shoulders at around −5 and –22 ppm (Fig. 5). The resonance at 0 ppm was the most intense peak and was attributed to free monomeric orthophosphate (e.g. free phosphoric acid or phosphorus oxides, not associated with alumina) [29,46,47]. The other resonances were attributed to different types of phosphorus in polyphosphate species. For example, the resonances at −5 and −11 ppm were assigned to phosphorus in the end groups and middle groups of polyphosphate chains, respectively [29,46]. Referring to coordination with alumina, the former can be assigned to P in pyrophosphoric acid or terminal groups of polyphosphates non-binding to Al, e.g. pyrophosphate ($H_4P_2O_7$) as well as orthophosphate binding to Al, e.g. Al-O-$P(OH)_3$ [46], which is similar to the peak at – 8 ppm in the case of alumina-based sample ($0.4P\text{-}Pt/Al_2O_3$ and $0.8P\text{-}Pt/Al_2O_3$), while the latter has been assigned to the branched polyphosphates with non-binding to Al, e.g. $H_5P_3O_{10}$ [46] or terminal groups of polyphosphates linked to Al [47]. The peak at –22 ppm was due to polymeric phosphate chains and condensed polyphosphates partially bonded to non-framework aluminum, e.g. $AlPO_4$ [46,47]; however, the very low intensity of this peak suggests a minor fraction of this coordination. Furthermore, the more intensive peaks at 0 and −11 ppm indicate substantial fractions of P in the forms of free monomeric phosphate (like H_3PO_4 and P_2O_5/P_4O_{10}) and middle groups of polyphosphate chains. A higher amount of free monomeric phosphate in zeolite than in alumina-based materials indicated that P interacted more weakly with the zeolite than alumina support.

To clarify the interaction of P and zeolites, ^{27}Al MAS NMR was performed to determine the coordination and local structure of

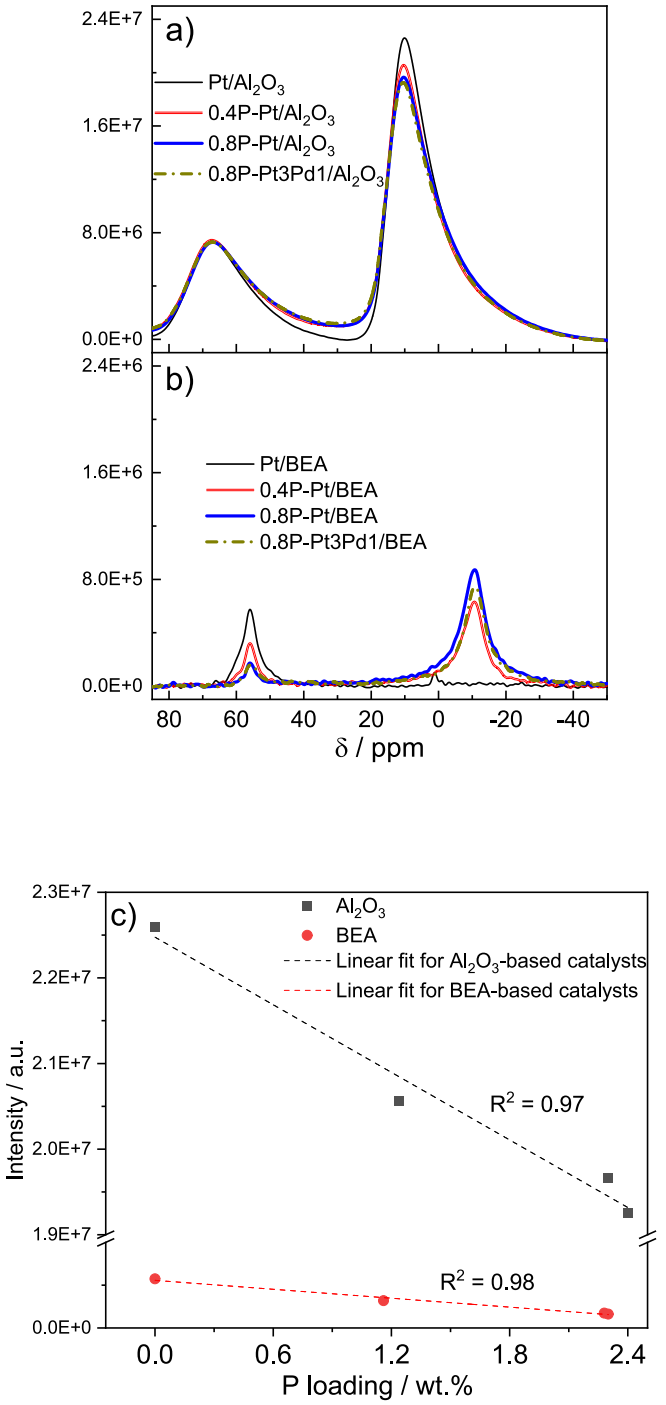

Fig. 6. ^{27}Al MAS NMR spectra of parent and phosphorus-impregnated catalysts (a, b) and the relationship between the intensity of the peak at around 10 ppm for four alumina-based samples (in Fig. 6a) and at 56 ppm for four zeolite-based samples (in Fig. 6b) and P loading (c).

aluminum in zeolite-based catalysts, and the spectra are shown in Fig. 6b. Noted that the scale of the y-axis of Fig. 6b is 10-fold smaller than Fig. 6a due to a lesser amount of aluminum in silica-rich zeolite than in alumina-based catalysts. The spectrum of Pt/BEA (no phosphorus) exhibited one strong peak at around 56 ppm and one weak peak at around 1 ppm. The former was assigned to the tetrahedral coordination of aluminum atoms in the framework of zeolites while the latter was attributed to the octahedral coordination of aluminum atoms in the extraframework of zeolites [29,48,49]. It is noted that the weak signal of the chemical shift around 1 ppm indicated a low number of Al in the extraframework which is a characteristic of dealuminated beta zeolites with high silica contents [49]. The ^{27}Al MAS NMR spectra of P-containing catalysts showed a substantial decrease of the signal at 56 ppm (Fig. 6b) and the decrement of the intensity of the peak is mostly linear with the P loading (Fig. 6c). Simultaneously, a new intense peak at around −10 ppm appeared and overlapped the peak at around 1 ppm. In the literature, this new chemical shift at −10 ppm has been assigned to a characteristic of octahedrally coordinated Al nuclei in aluminum phosphates [47,48]. A stronger intensity of the chemical shift at −10 ppm than at 56 ppm (Fig. 6b) indicated that the fraction of Al extracted from the zeolite framework to form $AlPO_4$ was larger than the one positioned in the framework after the incorporation of phosphorus. However, the total amount of $AlPO_4$ formation is relatively small because of the low aluminum content in the zeolite support (SiO_2/Al_2O_3 molar ratio of 217).

In summary, the NMR data revealed that the largest differences in the ^{31}P MAS NMR spectra between alumina-based and zeolite-based catalysts are the chemical shifts at 0 and –22 ppm. An intense peak at 0 ppm and a very weak peak at –22 ppm in the spectra of the zeolite-based materials suggests that when loading P in the zeolite-base catalysts, most of the phosphorus content existed in the form of phosphorus oxides and only a small fraction of phosphorus reacted with aluminum to form $AlPO_4$ outside of the zeolite framework.

NO-TPD measurements were performed to study the impact of P on the characteristics of NO adsorption on the catalysts, which may influence the conversion of NO under reaction conditions. Fig. 7 displays the desorption profile of NO and a correlation between the adsorbed amount of NO and the P loadings. The profile of NO desorption on Pt/BEA showed a broad peak from 40 to 160 °C with a desorption maximum of approximately 113 °C. This indicates a weak interaction between NO and Pt/BEA. The presence of P only caused a small decrease in the peak intensity, as a result, the desorption amount of NO decreased slightly from 8.9 μmol g^{-1} on Pt/BEA to 7.2 μmol g^{-1} on 0.8P-Pt/BEA (Table 1 and Fig. 7c). On the contrary, the desorption behavior of NO on Pt/Al_2O_3 was significantly different than for Pt/BEA. On the Pt/Al_2O_3, the desorption of NO occurred over a wide range of temperatures from 40 to 225 °C with a shoulder at approximately 113 °C and the main peak at 150 °C, which could be assigned to a weak and strong interaction between NO and Pt/Al_2O_3, respectively. The shoulder was increased slightly in the 0.4P-Pt/Al_2O_3 sample and it even became larger in the case of 0.8P-Pt/Al_2O_3. Notably, a second peak at a relatively high temperature of 320 °C was also observed in the profile for 0.8P-Pt/Al_2O_3. Moreover, the desorption amount of NO was slightly increased with an increase in the loading of P, from 11.9 μmol g^{-1} on Pt/Al_2O_3 to 15.8 μmol g^{-1} on 0.8P-Pt/Al_2O_3 (Table 1 and Fig. 7c), despite a slight decrease in the specific surface area with the presence of P. This indicated that the chemisorption of NO was more prominent than the physisorption on the series of P-Pt/Al_2O_3 catalysts. A similar trend in the shape of the NO-TPD profile and the desorption amount of NO was also observed for the degreening and P-poisoned Pt3Pd1/BEA and Pt3Pd1/Al_2O_3 catalysts, respectively (Fig. 7b and Table 1). To summarize, for the zeolite samples the NO desorption amount decreased, which could be related to the blocking of adsorption sites by the P_2O_5 which was the dominant species on the phosphorus-containing Pt/BEA (Fig. 3). Surprisingly, the NO adsorbed amount increased with the P content for the Pt/Al_2O_3 and Pt3Pd1/Al_2O_3 samples. Our results indicate that the NO could interact with the formed phosphate and phosphite species on the surface.

The interaction of the catalysts with CO probe molecules was investigated with CO adsorption to verify if the trend is similar to NO. The presence of P caused a decrease in the uptake of CO on both Pt/Al_2O_3 and Pt/BEA (Table 1). However, the Pt/BEA material was more sensitive to P than the Pt/Al_2O_3. For both studied loadings of P, the decrement in the uptake of CO was substantially larger for Pt/BEA than for Pt/Al_2O_3 (Fig. S12). For example, the amount of adsorbed CO on 0.8P-Pt/Al_2O_3 decreased by 36% compared to Pt/Al_2O_3, whereas the

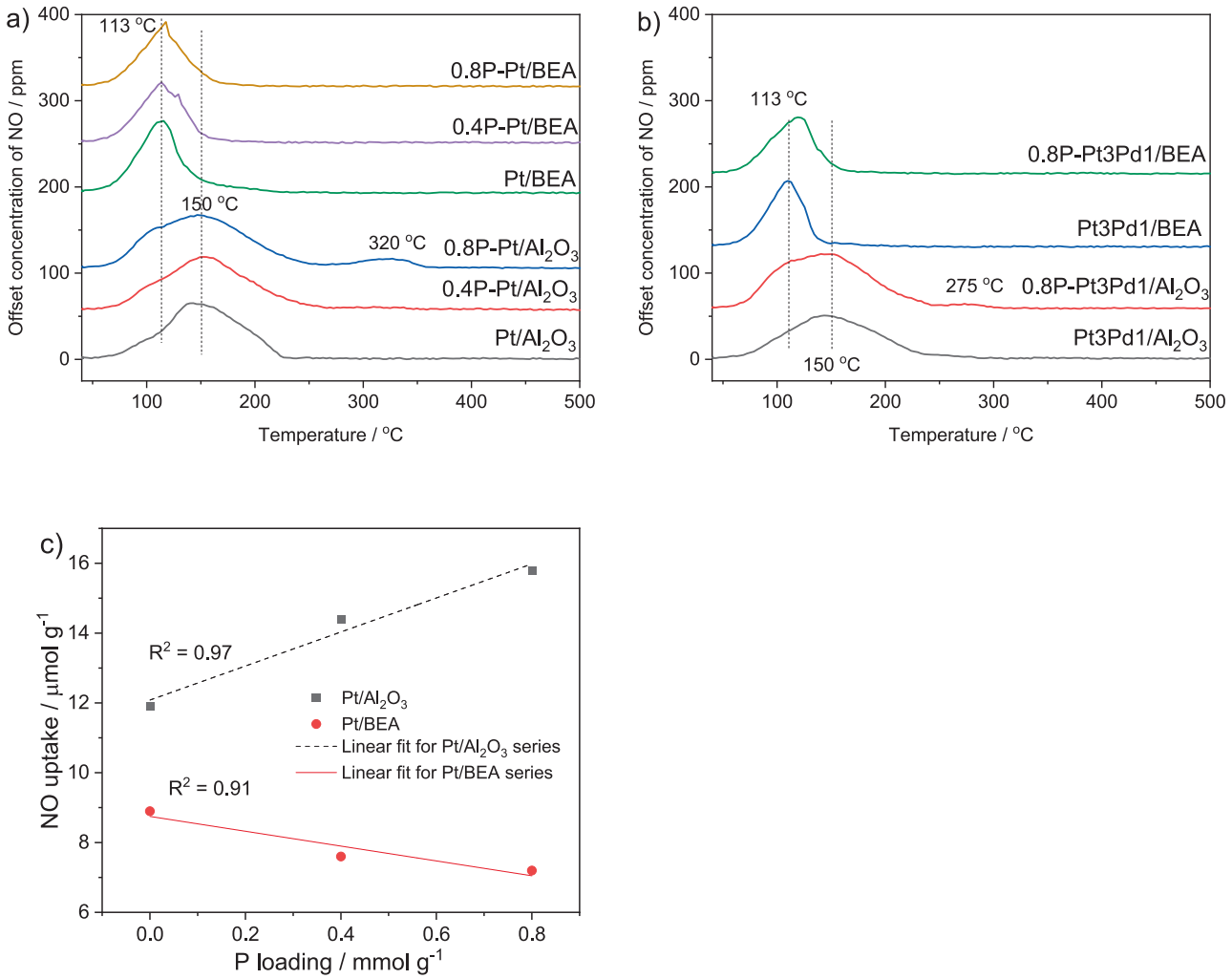

Fig. 7. a) Profiles of NO desorption on monometallic and b) bimetallic catalysts, and c) NO uptake correlation with P loading.

decrement of CO uptake between 0.8P-Pt/BEA and Pt/BEA was 69%. A decrease in the amount of CO chemisorption indicated a decrement in the accessible surface area of Pt sites. This could be related to the limited accessibility of the Pt sites and/or the sintering of Pt particles. Regarding the limited accessibility, it is suggested that P blocked the pores (entrance and/or inside) of the support and consequently limited the accessibility to all small Pt sites accommodated inside these pores. The blocking degree is more pronounced for the small pores (zeolite) than the large pores (alumina) and as a result, more Pt sites were blocked for 0.8P-Pt/BEA than 0.8P-Pt/Al_2O_3. Furthermore, the coverage of Pt particles on the outer surface (bigger than the pore size) should also be considered in both catalysts. However, it should be noted that the specific surface areas of 0.8P-Pt/Al_2O_3 and 0.8P-Pt/BEA decreased by only 12 and 20%, compared to Pt/Al_2O_3 and Pt/BEA, respectively. Therefore, these moderate decrements in the specific surface areas do not completely justify the significant drop in CO uptakes observed. It is also likely that some phosphorus species are directly adsorbed on the noble metal sites, and thereby poisoning the specific noble metal sites, and not blocking the whole pores. In addition, it is possible that the sintering of Pt may play a role. In both catalysts, phosphorus can react with alumina and decrease the acidity of the supports as anticipated by Al-NMR and this can cause more sintering of Pt particles due to a weaker metal-support interaction. This hypothesis was consistent with TEM data of Pt/Al_2O_3 since after P-impregnation the average size of Pt in Pt/Al_2O_3 increased by approximately 20%. In the case of zeolite catalysts, it is well known that the addition of phosphorus causes a decrease in acidity [48] by partial extraction of framework alumina to SAPO or $AlPO_4$ phases [22] or by "cationic exchange" and change of coordination in the framework from tetrahedral to octahedral positions [50]. This effect has been reported for zeolites with low Si/Al ratios (rich in aluminum) which also have less thermal stability. In the present work, to avoid the issue of thermal stability, a silica-rich beta zeolite (SiO_2/Al_2O_3 = 217) was employed. Therefore, the impact of P may be less pronounced. Indeed, no clear increase in the average size of Pt particles was observed from TEM data in this case.

3.2. *Effect of phosphorus poisoning*

The catalytic performance of each catalyst was tested for five sequential cycles (heating/cooling in a temperature range of 120 to 500 °C, heating rate of 5 °C min^{-1}). Prior to impregnation with $(NH_4)_2HPO_4$, the catalysts were pretreated by the degreening protocol to limit the effects of thermal aging on the interaction of P and noble metals.

3.2.1. *Monometallic Pt catalysts*

The results in Fig. 8 show a comparison of the oxidation of CO, NO, C_3H_8, and C_3H_6 for degreened monometallic Pt catalysts and those impregnated with 0.4 and 0.8 mmol P g^{-1} for the last cycle of five consecutive cycles. T_{50} (the temperatures at which the conversion reached 50%) of CO, C_3H_8, and C_3H_6 on each catalyst as well as the maximum conversion of NO oxidations are given in Table S1 and plotted

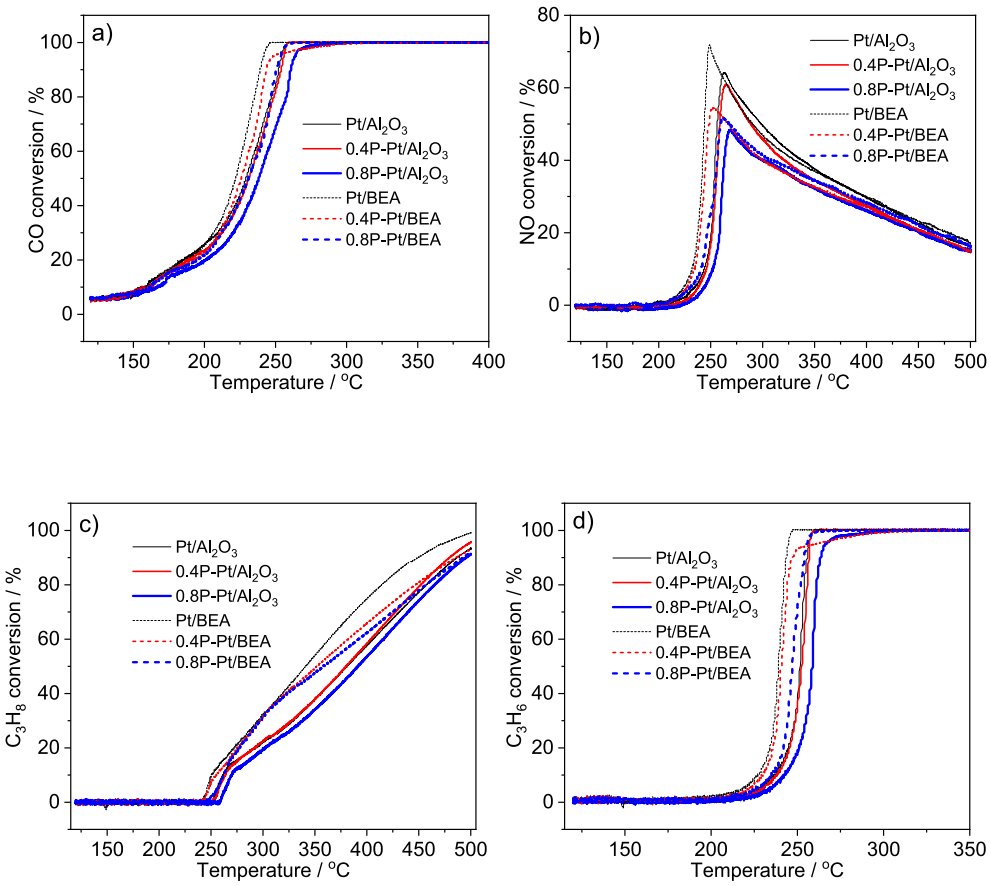

Fig. 8. Effect of P loadings on the conversion of a) CO, b) NO, c) C_3H_8 and d) C_3H_6 on monometallic Pt catalysts. Feed gas contains CO (1000 ppm), NO (500 ppm), C_3H_6 (500 ppm), C_3H_8 (500 ppm), O_2 (10 vol%), and H_2O (5 vol%) balanced in Ar.

in Fig. 9. Starting with the Pt/Al_2O_3 catalyst, the oxidation reactions commenced with the increasing order of T_{50} for different gases according to CO (229 °C) < C_3H_6 (252 °C) < NO (256 °C) < C_3H_8 (386 °C) (Fig. S13 and Table S1). A similar trend was also observed with the Pt/BEA sample (Fig. S13). However, all the T_{50} of CO, C_3H_6, NO, and C_3H_8 on Pt/BEA were shifted to lower values than those on Pt/Al_2O_3, showing that the Pt/BEA was more active than the Pt/Al_2O_3 catalyst. This is in line with the data reported in our previous work [24].

We start by examining the impact of P impregnation on the oxidation of CO. The presence of P showed a different effect on Pt/Al_2O_3 than Pt/BEA catalysts (Fig. 8a). The CO conversion profile for Pt/Al_2O_3 and 0.4P-Pt/Al_2O_3 was similar, whereas the one on 0.8P-Pt/Al_2O_3 was slightly shifted to a higher temperature. As a result, the increment in T_{50} (ΔT_{50}) compared to the Pt/Al_2O_3 was 2 °C and 9 °C for the 0.4P-Pt/Al_2O_3 and 0.8P-Pt/Al_2O_3, respectively. Furthermore, the CO conversion profile of the 0.8P-Pt/Al_2O_3 catalyst exhibited an additional feature in which the conversion rapidly increased to 97% at around 265 °C and then slowly reached full conversion at 300 °C. The turning point in this two-step profile coincided with the NO conversion maximum and the inflection point of the C_3H_6/C_3H_8 conversion profile (Fig. S13), suggesting that such inhibition of CO conversion at the second step might be caused by the co-feed with NO and hydrocarbons as reported in the literature [13]. It should be noted that the delay until reaching full conversion at around 265 °C can also be related to internal mass-transfer limitation to access the active sites due to the physical blockage of the active sites by phosphorus species. The impact of P on the CO conversion over Pt/BEA catalyst was observed even at a low loading of P, although the impact was small. The 0.4P-Pt/BEA showed a shift of the light-off curve toward higher temperature with a ΔT_{50} = 4 °C (Fig. 8a). The 0.8P-Pt/BEA sample had an ΔT_{50} = 9 °C, which was the same as that for the 0.8P-Pt/Al_2O_3 catalyst (Fig. 8a), suggesting that the degree of the impact was similar between the two types of catalysts at a high loading of P. These results are consistent with the CO chemisorption data (Table 1), which showed that the CO adsorption decreased significantly for 0.4P-Pt/BEA, but only slightly for 0.4P-Pt/Al_2O_3. This could be explained by the Pt/BEA catalyst being mainly physically blocked with P_2O_5 (XPS results, Fig. 3), which covers the surface and thereby both decreases the surface area and pore volume as well as hinders access to the active Pt sites.

The impact of P on the conversion of C_3H_6 was very similar to that for CO conversion in terms of the shape of the light-off curve (Fig. 8b) and ΔT_{50} (Fig. 9a). It is also worth noting that the T_{50} of both CO and C_3H_6 from the second to the fifth cycle of each catalyst with and without P did not change significantly (Table S1), suggesting that the presence of P did not induce substantially the oxidation of Pt with time-on-stream.

For C_3H_8 oxidation, both Pt/Al_2O_3 and 0.4P-Pt/Al_2O_3 showed a similar T_{50} of 386 °C while 0.8P-Pt/Al_2O_3 exhibited a T_{50} of 396 °C. Noticeably, the conversion profile of C_3H_8 on the 0.8P-Pt/Al_2O_3 was quite consistent with that on the Pt/Al_2O_3 but it was shifted toward a higher temperature. This suggests that the presence of P seemed to block a fraction of the Pt sites and the degree of the blockage did not change with an increase in temperature from 250 to 500 °C, wherein the oxidation of C_3H_8 occurred. In contrast, over the Pt/BEA series, the addition of P strongly impacted C_3H_8 oxidation even at a low loading; the increment of T_{50} was 12 and 19 °C for 0.4P-Pt/BEA and 0.8P-Pt/BEA, respectively. Moreover, the decrease in the conversion of C_3H_8 on the P-containing zeolite catalyst was substantial at temperatures higher than approximately 325 °C indicating that the inhibition of P on the C_3H_8 oxidation on the Pt/BEA series was more severe at high temperatures.

Clearly, a significant drop of T_{50} on P-impregnated zeolite could be

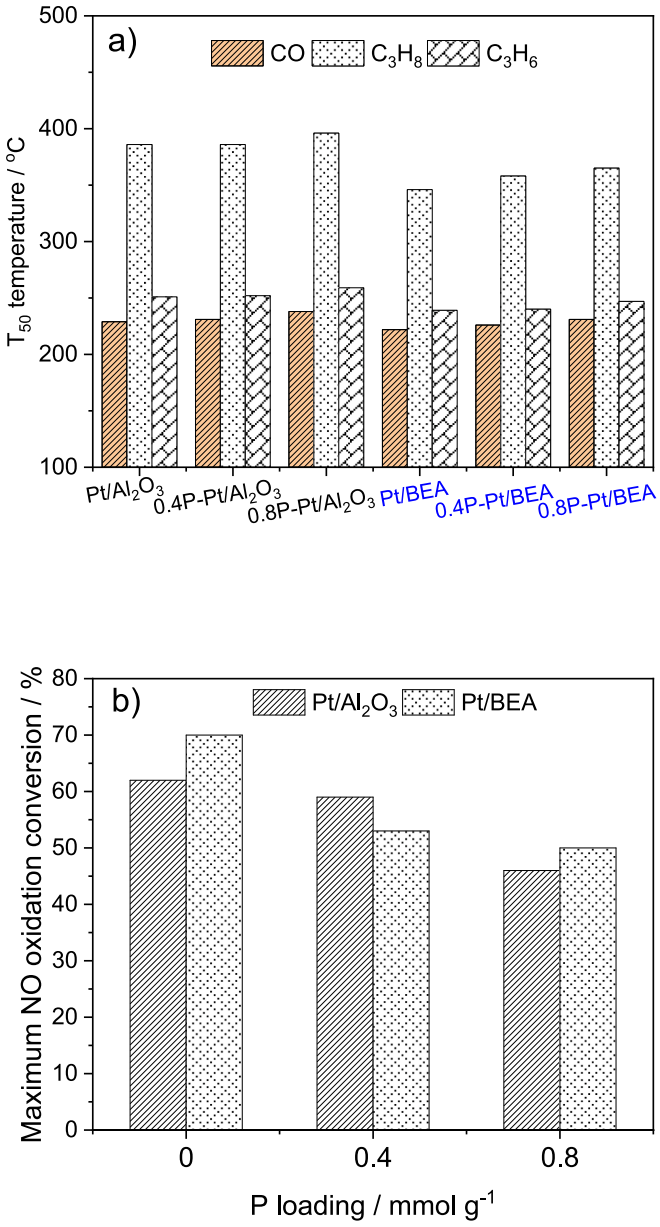

Fig. 9. a) Dependence of T_{50} temperature for CO, C_3H_6, and C_3H_8 and b) maximum conversion of NO on monometallic Pt catalysts with different P loadings.

more affected by pore restrictions. In order to examine if the calcination and pre-treatment after the P addition could induce Pt sintering due to the decrease in Brönsted acidity by P impregnation, we carried out two extra experiments. These experiments on both Pt/BEA-2 and 0.8P-Pt/BEA-2 were conducted with the addition of the degreening (thermal treatment at 700 °C in NO, O_2, and H_2O) and the pretreatment (500 °C) of the monoliths before feeding the reactants. Thus, these samples have a degreening both before the addition of phosphorus on the powder catalysts as well as before the pre-treatment started on the monoliths. Note that these two samples are the same as Pt/BEA-1 and 0.8P-Pt/BEA-1 catalysts, and the only difference is that these monoliths were treated under degreening and pretreatment conditions. As shown in Fig. S14c, the profiles of C_3H_8 conversion of the 0.8P-Pt/BEA-2 catalyst shifted to a higher temperature than that of the 0.8P-Pt/BEA-1 catalyst, as a result, the increment of T_{50} (ΔT_{50}) was approximately 12 °C, which was due to the extra pre-treatment. It should be noted that without P-impregnation, the Pt/BEA catalysts showed no difference in T_{50} between the tests without and with the degreening step. Thus, the addition of P resulted in an increased deactivation during pre-treatment of the monoliths after P impregnation. This could be a result of an induced sintering due to the removal of acid sites after P impregnation. However, the increment of T_{50} was similar for the sample without and with phosphorus impregnation with the tests where the degreening was included compared to the one without for CO, NO, and C_3H_6 oxidation (Fig. S14 a, b, d). Thus, the effect of pre-treatment is not the same for different oxidation reactions, suggesting a complex mechanism.

For NO oxidation, the presence of P not only lowered the maximum conversion of NO but also slightly increased the temperatures at which the maximum conversions were achieved. The impact of P-poisoning on NO conversion is substantially different between Pt/Al_2O_3 and Pt/BEA catalysts. For the fifth cycle, the maximum conversion of NO decreased slightly from 62% on Pt/Al_2O_3 to 59% on 0.4P-Pt/Al_2O_3 and significantly to 46% on 0.8P-Pt/Al_2O_3, whereas the maximum conversion of NO dropped substantially from 70% on Pt/BEA to 53% on 0.4P-Pt/BEA and to 50% on 0.8P-Pt/BEA. The same low loading of P of 0.4 mmol g^{-1} caused a drop of maximum conversion of NO by only 3% for Pt/Al_2O_3 but it was 17% for Pt/BEA. This indicated that Pt/BEA was more susceptible to phosphorus poisoning than Pt/Al_2O_3. Alumina in Pt/Al_2O_3 can act as a reservoir to capture phosphorus (e.g. phosphate) and lower the formation of P_2O_5 which can block the Pt sites. This subsequently assisted to maintain the high conversion of NO for the 0.4P-Pt/Al_2O_3 catalyst. For 0.8P-Pt/Al_2O_3, the amount of P is high enough to further block the Pt sites (after a part of P was captured by alumina) and hence decreased the maximum conversion of NO. For Pt/BEA, the phosphorus compounds had weak interaction with the zeolite (unlike the alumina support) and thus even with a low loading of P, the phosphorus compounds tended to both block the pores of zeolites (containing some small Pt particles inside) and surround the Pt sites on the outer surface of the zeolites. As a result, the available sites of Pt decreased and subsequently inhibited significantly the maximum conversion of NO for 0.4P-Pt/BEA catalyst. Increasing loading of P (0.8 mmol g^{-1}) resulted in even more pore blockage and Pt surrounding and thereafter caused a further drop of the maximum conversion of NO on 0.8P-Pt/BEA catalyst. It should be also noted that NO oxidation is a thermodynamic-limited reaction with a decreasing NO_2 concentration when increasing the temperature. Moreover, at lower temperatures the NO oxidation reaction is often limited by the kinetics, resulting in that the NO_2 profile usually is volcano-shaped. In the NO conversion profiles of phosphorus-containing catalysts, the temperatures for maximum conversions of NO are shifted to a higher temperature than that of the phosphorus-free catalyst, and the thermodynamic limitation may therefore lower the maximum conversion. In the other words, the thermodynamic limit is also a possible reason for the decreased maximum conversion of NO on the phosphorus-containing catalysts. Last but not least, the effect of CO-SCR and hydrocarbon-SCR on the conversion of NO could not be discarded as reported in our previous work [24].

3.2.2. *Bimetallic Pt-Pd catalysts*

High loading of P (0.8 mmol g^{-1} or 2.4 wt%) was used to investigate the effect of P on the catalytic activity of bimetallic catalysts including $Pt3Pd1/Al_2O_3$ and Pt3Pd1/BEA. Fig. 10 compares the CO, NO, C_3H_8, and C_3H_6 conversions on the parent and P-impregnated catalysts, while Fig. 11 shows the difference in T_{50} values of CO, C_3H_6, and C_3H_8 conversions and maximum conversion of NO. For CO oxidation, the T_{50} for the fifth cycle of the 0.8P-$Pt3Pd1/Al_2O_3$ was 170 °C, which was only 3 °C higher than that of the $Pt3Pd1/Al_2O_3$. In contrast, the 0.8P-Pt3Pd1/BEA exhibited a T_{50} of 179 °C, which was 12 °C higher than that of the phosphorus-free sample, Pt3Pd1/BEA (Fig. 11a). Such a larger increment of T_{50} on the zeolite-based catalyst than the alumina-based indicated that the impregnation of P more strongly impacted the former than the latter, in the same way as for Pt-based catalysts. Moreover, for the 0.8P-Pt3Pd1/BEA, CO conversion increased rapidly to 95–96% at around 215 °C and then slowly increased the conversion, with a full

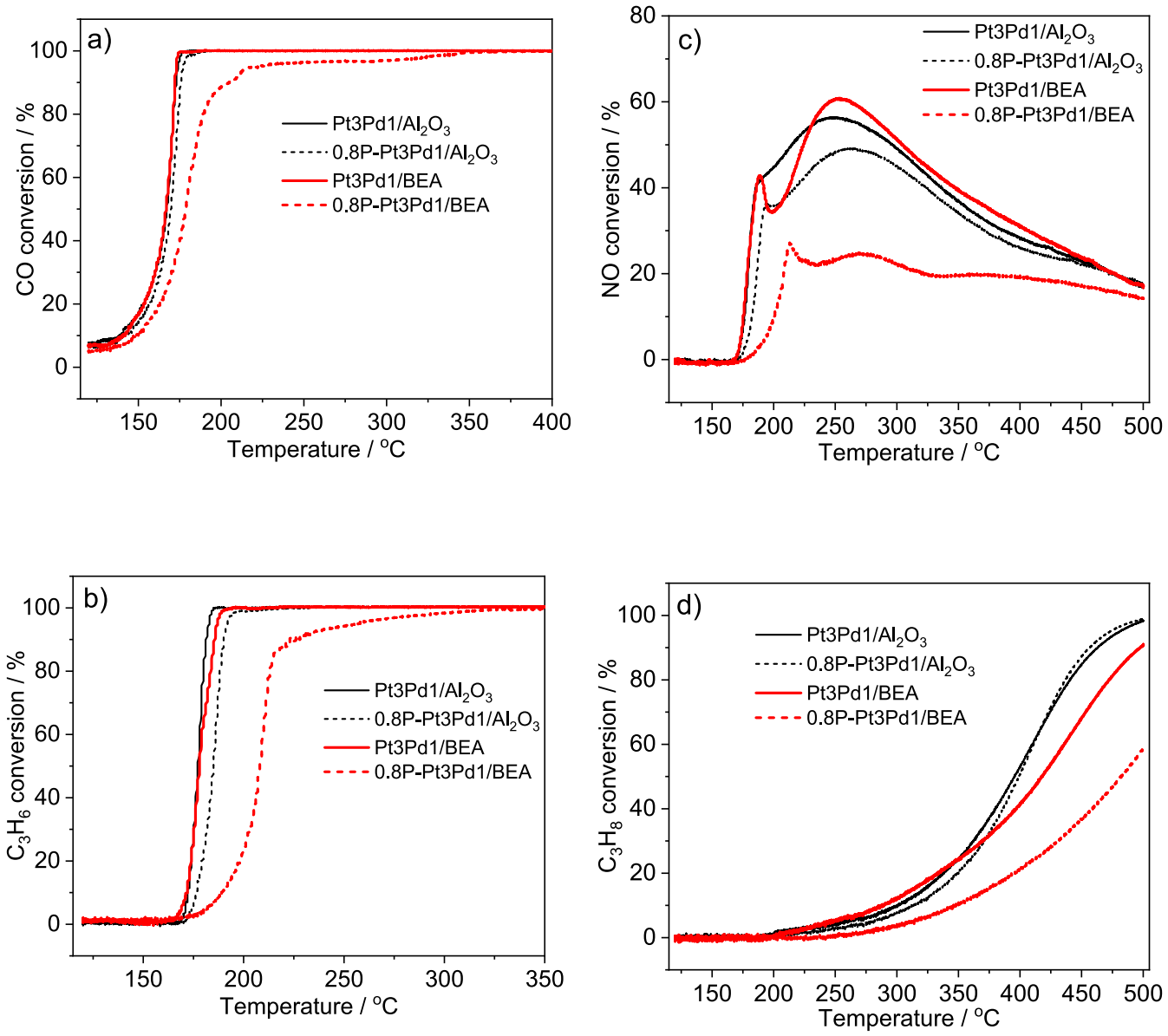

Fig. 10. Effect of P loadings on the conversion of a) CO, b) C_3H_6, c) NO, and d) C_3H_8 on bimetallic Pt3Pd1 catalysts. Feed gas contains CO (1000 ppm), NO (500 ppm), C_3H_6 (500 ppm), C_3H_8 (500 ppm), O_2 (10 vol%), and H_2O (5 vol%) balanced in Ar.

conversion at around 370 °C (Fig. 10a). A similar phenomenon was also observed for the conversion of CO on the 0.8P-Pt3Pd1/Al_2O_3 catalyst in which the conversion quickly reached 98% at 180 °C and then slowly increased to 100% at 200 °C. This characteristic stepwise conversion of CO on the catalysts poisoned with P has been also reported in the literature [13]. Agote-Arán and coworkers found that a Pt-Pd /Al_2O_3 catalyst containing 2.5 wt% P loading exhibited a temperature window of 180–325 °C for the delay of the CO conversion from 97% to 100%. Moreover, the propene conversion profile exhibited a similar delay in conversion at higher temperatures (Fig. 10b), where the conversion increased to around 90% at 225 °C and then slowly increased to reach complete oxidation of C_3H_6 at around 340 °C. In addition, NO oxidation was also significantly influenced in this sample. A possible reason for this effect could be that the 0.8P-Pt3Pd1/BEA sample has significant physical blocking of phosphorous species as evident from the large drop in the specific surface area (Table 1). This could result in increased internal mass-transfer resistance and thereby, a lower apparent activation energy for higher temperatures.

The T_{50} of C_3H_6 oxidation on 0.8P-Pt3Pd1/BEA was 30 °C higher than that of the phosphorus-free counterpart (Fig. 11a). Meanwhile, the 0.8P-Pt3Pd1/Al_2O_3 catalyst had an increment of T_{50} of only about 7 °C compared to the Pt3Pd1/Al_2O_3 catalyst. A lower increment of T_{50} for the 0.8P-Pt3Pd1/Al_2O_3 catalyst than for the 0.8P-Pt3Pd1/BEA and 0.8P-Pt1Pd1/BEA catalysts indicated a less severe poisoning of P on the alumina-based catalyst than the zeolite-based ones. This was the same result as for the Pt/Al_2O_3 and Pt/BEA and can be related to the different types of phosphorus poisoning (physical versus chemical poisoning).

The NO conversion profiles on the degreened bimetallic catalysts (Pt3Pd1/Al_2O_3 and Pt3Pd1/BEA) had two peaks including one sharp peak at around 190 °C due to the reduction with hydrocarbons and one broad peak at around 255 °C (Fig. 10c) due to the oxidation of NO, as observed in our previous study [26]. Loading with P caused not only a substantial decrease in the NO conversion but also a shift of T_{max} (the temperature at which the conversion by the reduction and the oxidation reached maximum values) to higher temperatures (Fig. 10c). For example, the T_{max} for the 0.8P-Pt3Pd1/Al_2O_3 and 0.8P-Pt3Pd1/BEA was shifted to approximately 10 and 20 °C higher than the Pt3Pd1/Al_2O_3 and 0.8P-Pt3Pd1/BEA, respectively (Fig. 11b). Also, the maximum

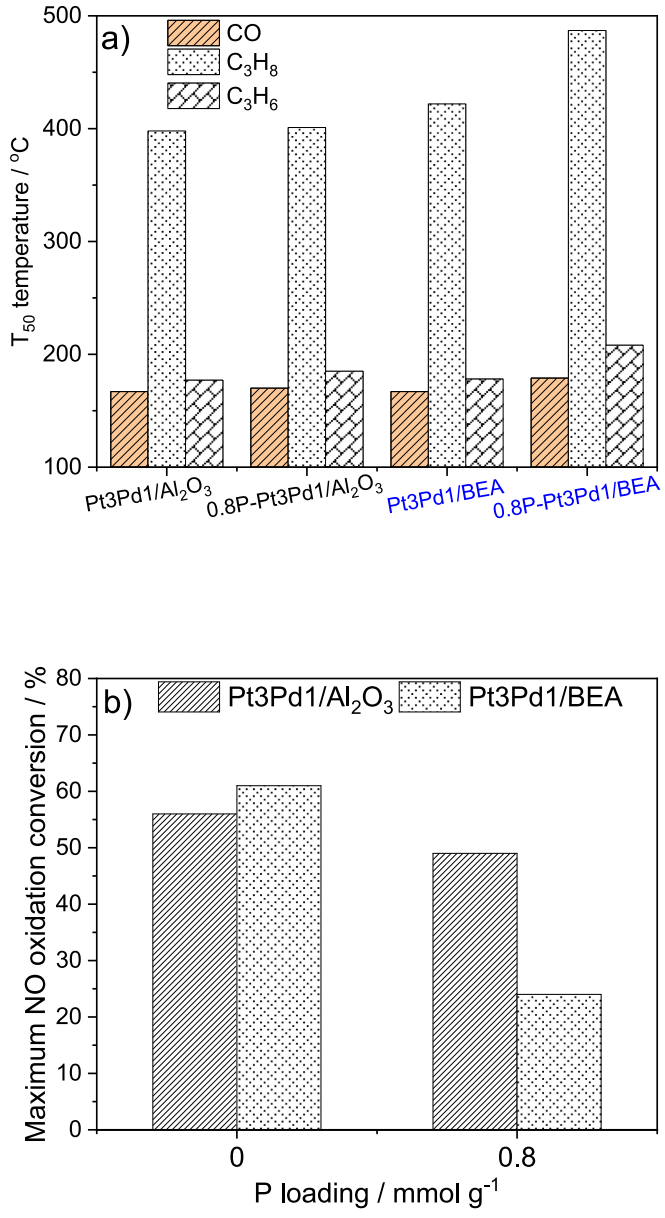

Fig. 11. a) Dependence of T_{50} temperature for CO, C_3H_6, and C_3H_8 and b) maximum conversion of NO on bimetallic Pt3Pd1 catalysts with different P loadings.

conversion of NO oxidation decreased from 56 to 49% for $Pt3Pd1/Al_2O_3$ and 61 to 24% for 0.8P-Pt3Pd1/BEA after loading with 0.8 mmol g^{-1} of P. A significant loss of the maximum conversion on Pt3Pd1/BEA compared to $Pt3Pd1/Al_2O_3$ after loading P indicated that the impact of P poisoning is more pronounced for zeolite than alumina-based catalysts, and this trend is similar to that for monometallic Pt catalysts.

The P inhibition for C_3H_8 oxidation was very different for $Pt3Pd1/Al_2O_3$ and Pt3Pd1/BEA. The 0.8P-$Pt3Pd1/Al_2O_3$ and 0.8P-Pt3Pd1/BEA exhibited T_{50} of C_3H_8 around 400 and 480 °C (Fig. 10d), which was 5 °C and 65 °C higher than those for the P-free counterparts (Fig. 11a). The change in the conversion profiles during the five-cycle tests is another interesting point to evaluate the impact of P. A difference in poisoning characteristics might be related to the interaction of P and the support. For zeolite-based catalysts, P interacted weaker with zeolite support as the major part of the phosphorus was in the form of P_2O_5 on the surface of zeolites, which could block the noble metal sites or the accessibility to them. Whereas for alumina-based catalysts, P interacts strongly with the alumina support, as evident from the XPS measurements (Fig. 3) and this could result in more of the noble metal sites being active. This is also consistent with the CO chemisorption results (Table 1), where the dispersion decreased significantly after poisoning the BEA-supported catalysts. Therefore, a significant decrease in the textural properties of the zeolite-based materials due to P-poisoning could explain a more severe decrease in the catalytic performance of the zeolite-based materials than their alumina-based counterparts.

The five conversion profiles of C_3H_8 for 0.8P-Pt3Pd1/BEA were almost identical during the five-cycle tests, although the profiles for 0.8P-Pt3Pd1/BEA were shifted to a higher temperature than those for Pt3Pd1/BEA (Figs. S15 and S16). This suggests that the loading of P caused poisoning and subsequently decreased the number of active sites; however, these active sites were quite stable with time-on-stream. By contrast, the conversion profiles of C_3H_8 for $Pt3Pd1/Al_2O_3$ and 0.8P-$Pt3Pd1/Al_2O_3$ were slightly shifted to higher temperatures after each cycle during the five-cycle tests (Figs. S17 and S18). This indicates that the activity decreased gradually after each cycle. The increased light-of temperature, especially for C_3H_8 oxidation, for degreened $Pt3Pd1/Al_2O_3$ could be due to gradual oxidation with time-on-stream after each cycle which was consistent with our previous study [24]. The oxidation of the active sites is likely related to Pd-Pt alloying because the increment of T_{50} was not observed clearly in the case of monometallic catalysts (see Table S1). Interestingly, for 0.8P-$Pt3Pd1/Al_2O_3$ the activity was more stable after repeated cycles (Fig. S18) compared to $Pt3Pd1/Al_2O_3$ (Fig. S17).

To summarize, phosphorus poisoning resulted in a decrease in the catalytic activity and it was more pronounced on zeolite-based catalysts than alumina-based ones. The reasons for this could be seen from the characterization results where the impregnated phosphorous interacted with the alumina and high-siliceous content zeolite beta in different ways. A stronger interaction between P and the alumina than zeolite was observed, which resulted in the formation of phosphate compounds for the former but a prominent amount of free phosphorus oxide (P_2O_5/P_4O_{10}) in the latter. The phosphorus compounds block partially the pore of the supports and this decreased the specific surface areas of the catalysts. However, the decrement was more severe for the zeolite-based than the alumina-based catalysts, which could be due to the formation of a high fraction of P_2O_5 on the BEA samples. The phosphorus species can block the entrance of the pores or fill in the pores which hosted some small Pt particles inside and thereby block the accessibility to those small Pt particles. Also, the phosphorus species can adsorb on the large particles of Pt on the external surface of the supports (outside of the pores). The presence of P seemed not to influence the oxidation state of the Pt species, but it decreased the available surface of the Pt active sites. As a result, the adsorption capacity of the P-containing catalysts for CO was lower than the fresh catalysts, especially for the BEA-containing samples due to the pore blockage and phosphorus adsorption on Pt. The lower amount of available noble metal sites after poisoning for the BEA samples compared to Al_2O_3 samples could explain the more severe effect of P on the hydrocarbon light off.

4. Conclusions

Two series of monometallic Pt and bimetallic PtPd supported on alumina and beta zeolite ($SiO_2/Al_2O_3 = 217$) were artificially poisoned with phosphorus (1.2 and 2.4 wt%) by impregnation. The textural property of the catalysts was significantly influenced by the presence of phosphorus even at a low P content. The decrement in the values of the specific surface areas was linearly proportional with the loading of P; however, the effect was more pronounced for the zeolite than the alumina-based catalysts. Poisoning with 2.4 wt% P caused a decrease of 12–15% of the specific surface area for the alumina-based catalyst, while the surface area for the zeolite samples decreased by about 30–32%. P interacted with the alumina and beta zeolite supports in different ways. Phosphate was observed for alumina-based catalysts, while both

phosphorus oxides (P_2O_5/P_4O_{10}) and phosphates were found for the zeolite-based catalysts. During the calcination, phosphorus precursor $(NH_4)_2HPO_4$ decomposed into different intermediate products, e.g. H_3PO_4 and $H_2P_4O_7$, and these compounds can react with alumina support to form phosphate/polyphosphate or can dehydrate to form phosphorus oxides (P_2O_5/P_4O_{10}). In the case of zeolite-based catalysts (high-silica content as used in this study), only a small fraction of $AlPO_4$ was formed and most phosphorus species existed in form of oxides. Whereas, in the cases of alumina-based catalysts, most phosphorus intermediates reacted with alumina (abundant) to form $AlPO_4$. The ^{31}P NMR data, which is a bulk analytical technique confirmed a high fraction of free phosphorus oxides (e.g. P_2O_5 and P_4O_{10}) in the zeolite-based catalysts and a dominant percentage of formed phosphate for the alumina-based samples. A large fraction of phosphorus oxides on zeolites can block the entrance of the pores or fill in the pores which hosted some small Pt particles inside and therefore the accessibility to those small Pt particles was hindered. Also, the phosphorus species can attach on large particles of Pt on the external surface of the supports (outside of the pores). In the cases of alumina-based catalysts, most of the P reacted with the alumina support and only some of the P covered the active sites. Hence the decrease in the number of available active sites was more significant for zeolite- than alumina-based catalysts which also was observed in CO chemisorption experiments. As a result, the presence of P caused a decrease in the catalytic performance of the catalysts for the oxidation of all four components (CO, NO, C_3H_6 and C_3H_8) and the inhibition of P on the activity was more pronounced for zeolite-based than alumina-based diesel oxidation catalysts.

Author contribution

Concepts and design of experiments: P.H.H., L.O.; Experiments and characterizations: P.H.H., J.S., D.Y., W.D.; Write a draft manuscript: P. H.H. Edit manuscript: D.C. and L.O., Funding management: L.O. All authors discussed the data and contributed to the manuscript.

Declaration of Competing Interest

The authors declare the following financial interests/personal relationships which may be considered as potential competing interests: Louise Olsson is one of the editors for Chemical Engineering Journal.

Data availability

Data will be made available on request.

Acknowledgments

This work was performed at the Competence Catalysis Center (KCK) and the Division of Chemical Engineering. The authors gratefully acknowledge the Swedish Energy Agency, Johnson Matthey, and Volvo AB for financial support via the FFI project (Grant number 48038-1). We would like to thank Dr. Lennart Andersson, Dr. Martin Petersson (Volvo AB) and Dr. Gudmund Smedler, Dr. Francois Moreau, Dr. Andrew Chiffey (Johnson Matthey) for their valuable comments and discussions. We also appreciate Dr. Eric Tam for XPS measurements; Dr. Andreas Schaefer for CO chemisorption measurements, and Dr. Tobias Sparrman for his assistance in solid-state NMR analysis. The Swedish NMR centre node at Umeå University is acknowledged for support.

Appendix A. Supplementary data

Supplementary data to this article can be found online at https://doi.org/10.1016/j.cej.2023.143548.

References

[1] A. Wang, L. Olsson, The impact of automotive catalysis on the United Nations sustainable development goals, Nat. Catal. 2 (2019) 566–570.
[2] C. Ciardelli, I. Nova, E. Tronconi, D. Chatterjee, B. Bandl-Konrad, M. Weibel, B. Krutzsch, Reactivity of NO/NO2–NH3 SCR system for diesel exhaust aftertreatment: Identification of the reaction network as a function of temperature and NO2 feed content, Appl. Catal. B 70 (1-4) (2007) 80–90.
[3] M. Seneque, F. Can, D. Duprez, X. Courtois, NOx Selective Catalytic Reduction (NOx-SCR) by Urea: Evidence of the Reactivity of HNCO, Including a Specific Reaction Pathway for NOx Reduction Involving NO + NO2, ACS Catal. 6 (7) (2016) 4064–4067.
[4] A. Russell, W.S. Epling, Diesel Oxidation Catalysts, Catal. Rev. 53 (4) (2011) 337–423.
[5] T.R. Johns, J.R. Gaudet, E.J. Peterson, J.T. Miller, E.A. Stach, C.H. Kim, M. P. Balogh, A.K. Datye, Microstructure of Bimetallic Pt•Pd Catalysts under Oxidizing Conditions, ChemCatChem 5 (9) (2013) 2636–2645.
[6] A. Stanislaus, A. Marafi, M.S. Rana, Recent advances in the science and technology of ultra low sulfur diesel (ULSD) production, Catal. Today 153 (2010) 1–68.
[7] A.K. Neyestanaki, F. Klingstedt, T. Salmi, D.Y. Murzin, Deactivation of postcombustion catalysts, a review, Fuel 83 (2004) 395–408.
[8] W. Yang, J. Gong, X. Wang, Z. Bao, Y. Guo, Z. Wu, A Review on the Impact of SO2 on the Oxidation of NO, Hydrocarbons, and CO in Diesel Emission Control Catalysis, ACS Catal. 11 (20) (2021) 12446–12468.
[9] B.G. Bunting, K. More, S. Lewis, T. Toops, Phosphorous Poisoning and Phosphorous Exhaust Chemistry with Diesel Oxidation Catalysts, SAE Int. (2005).
[10] P. Anguita, F. Gaillard, E. Iojoiu, S. Gil, A. Giroir-Fendler, Study of hydrothermal aging impact on Na- and P-modified diesel oxidation catalyst (DOC), J. Catal. 375 (2019) 329–338.
[11] P. Lott, M. Eck, D.E. Doronkin, A. Zimina, S. Tischer, R. Popescu, S. Belin, V. Briois, M. Casapu, J.-D. Grunwaldt, O. Deutschmann, Understanding sulfur poisoning of bimetallic Pd-Pt methane oxidation catalysts and their regeneration, Appl. Catal. B 278 (2020), 119244.
[12] M. Agote-Arán, M. Elsener, F.W. Schütze, C.M. Schilling, M. Sridhar, E. Katsaounis, O. Kröcher, D. Ferri, On the relevance of P poisoning in real-world DOC aging, Appl. Catal. B 291 (2021), 120062.
[13] M. Agote-Arán, M. Elsener, F.W. Schütze, C.M. Schilling, M. Sridhar, E. Katsaounis, O. Kröcher, D. Ferri, Understanding the impact of poison distribution on the performance of Diesel oxidation catalysts, Appl. Catal. B 299 (2021) 120684.
[14] A. Wang, J. Wang, S. Sheti, S. Dahlin, J. Han, J. Woo, K. Xie, L.J. Pettersson, L. Olsson, A deactivation mechanism study of phosphorus-poisoned diesel oxidation catalysts: model and supplier catalysts, Catal. Sci. Technol. 10 (16) (2020) 5602–5617.
[15] P. Anguita, J.M. García-Vargas, F. Gaillard, E. Iojoiu, S. Gil, A. Giroir-Fendler, Effect of Na, K, Ca and P-impurities on diesel oxidation catalysts (DOCs), Chem. Eng. J. 352 (2018) 333–342.
[16] M.J. Rokosz, A.E. Chen, C.K. Lowe-Ma, A.V. Kucherov, D. Benson, M.C. Paputa Peck, R.W. McCabe, Characterization of phosphorus-poisoned automotive exhaust catalysts, Appl. Catal. B 33 (2001) 205–215.
[17] S.K. Matam, E.V. Kondratenko, M.H. Aguirre, P. Hug, D. Rentsch, A. Winkler, A. Weidenkaff, D. Ferri, The impact of aging environment on the evolution of Al2O3 supported Pt nanoparticles and their NO oxidation activity, Appl. Catal. B 129 (2013) 214–224.
[18] A. Winkler, D. Ferri, M. Aguirre, The influence of chemical and thermal aging on the catalytic activity of a monolithic diesel oxidation catalyst, Appl. Catal. B 93 (2009) 177–184.
[19] V. Kröger, T. Kanerva, U. Lassi, K. Rahkamaa-Tolonen, M. Vippola, R.L. Keiski, Characterization of phosphorus poisoning on diesel exhaust gas catalyst components containing oxide and Pt, Top. Catal. 45 (2007) 153–157.
[20] M. Honkanen, M. Kärkkäinen, O. Heikkinen, K. Kallinen, T. Kolli, M. Huuhtanen, J. Lahtinen, R.L. Keiski, T. Lepistö, M. Vippola, The Effect of Phosphorus Exposure on Diesel Oxidation Catalysts—Part II: Characterization of Structural Changes by Transmission Electron Microscopy, Top. Catal. 58 (2015) 971–976.
[21] M. Honkanen, M. Huuhtanen, M. Kärkkäinen, T. Kanerva, K. Lahtonen, A. Väliheikki, K. Kallinen, R.L. Keiski, M. Vippola, Characterization of Pt-based oxidation catalyst – Deactivated simultaneously by sulfur and phosphorus, J. Catal. 397 (2021) 183–191.
[22] H.E. van der Bij, B.M. Weckhuysen, Phosphorus promotion and poisoning in zeolite-based materials: synthesis, characterisation and catalysis, Chem. Soc. Rev. 44 (20) (2015) 7406–7428.
[23] P.H. Ho, J. Woo, R.F. Ilmasani, M.A. Salam, D. Creaser, L. Olsson, The Effect of Si/Al Ratio on the Oxidation and Sulfur Resistance of Beta Zeolite-Supported Pt and Pd as Diesel Oxidation Catalysts, ACS Eng. Au 2 (1) (2022) 27–45.
[24] P.H. Ho, D. Yao, D. Creaser, L. Olsson, Advantages of High-Siliceous Zeolites in the Reactivity and Stability of Diesel Oxidation Catalysts, ACS Eng. Au (2022).
[25] P.H. Ho, J.-W. Woo, R. Feizie Ilmasani, J. Han, L. Olsson, The role of Pd–Pt Interactions in the Oxidation and Sulfur Resistance of Bimetallic Pd–Pt/γ-Al2O3 Diesel Oxidation Catalysts, Ind. Eng. Chem. Res. 60 (18) (2021) 6596–6612.
[26] P.H. Ho, J. Shao, D. Yao, R.F. Ilmasani, M.A. Salam, D. Creaser, L. Olsson, The effect of Pt/Pd ratio on the oxidation activity and resistance to sulfur poisoning for Pt-Pd/BEA diesel oxidation catalysts with high siliceous content, J. Environ. Chem. Eng. 10 (2022), 108217.
[27] M. Statheropoulos, S.A. Kyriakou, Quantitative thermogravimetric-mass spectrometric analysis for monitoring the effects of fire retardants on cellulose pyrolysis, Anal. Chim. Acta 409 (2000) 203–214.

[28] A. Marcilla, M.I. Beltran, A. Gómez-Siurana, I. Martinez-Castellanos, D. Berenguer, V. Pastor, A.N. García, TGA/FTIR study of the pyrolysis of diammonium hydrogen phosphate–tobacco mixtures, J. Anal. Appl. Pyrol. 112 (2015) 48–55.
[29] M. Göhlich, W. Reschetilowski, S. Paasch, Spectroscopic study of phosphorus modified H-ZSM-5, Microporous Mesoporous Mater. 142 (2011) 178–183.
[30] J. Quartararo, M. Guelton, M. Rigole, J.-P. Amoureux, C. Fernandez, J. Grimblot, Sol–gel synthesis of alumina modified by phosphorus: a solid state NMR characterization study, J. Mater. Chem. 9 (1999) 2637–2646.
[31] F. Cabello Galisteo, C. Larese, R. Mariscal, M. López Granados, J.L.G. Fierro, R. Fernández-Ruiz, M. Furió, Deactivation on vehicle-aged diesel oxidation catalysts, Top. Catal. 30 (2004) 451–456.
[32] M. Kärkkäinen, T. Kolli, M. Honkanen, O. Heikkinen, M. Huuhtanen, K. Kallinen, T. Lepistö, J. Lahtinen, M. Vippola, R.L. Keiski, The Effect of Phosphorus Exposure on Diesel Oxidation Catalysts—Part I: Activity Measurements, Elementary and Surface Analyses, Top. Catal. 58 (2015) 961–970.
[33] K. Ramesh, L.M. Hui, Y.-F. Han, A. Borgna, Structure and reactivity of phosphorous modified H-ZSM-5 catalysts for ethanol dehydration, Catal. Commun. 10 (2009) 567–571.
[34] B. Wang, X. Yan, H. Zhang, Interaction between phosphorus and zeolite/binder: A realumination study on beta zeolites, Microporous Mesoporous Mater. 312 (2021) 110735.
[35] Z. Chen, C. Bian, Y. Guo, L. Pang, T. Li, Efficient Strategy to Regenerate Phosphorus-Poisoned Cu-SSZ-13 Catalysts for the NH3-SCR of NOx: The Deactivation and Promotion Mechanism of Phosphorus, ACS Catal. 11 (2021) 12963–12976.
[36] G.W. Graham, H.-W. Jen, O. Ezekoye, R.J. Kudla, W. Chun, X.Q. Pan, R. W. McCabe, Effect of alloy composition on dispersion stability and catalytic activity for NO oxidation over alumina-supported Pt–Pd catalysts, Catal. Lett. 116 (1-2) (2007) 1–8.
[37] D.E. Newbury, Mistakes Encountered during Automatic Peak Identification in Low Beam Energy X-ray Microanalysis, Scanning 29 (4) (2007) 137–151.
[38] T. Lindblad, B. Rebenstorf, Z.-G. Yan, S.L.T. Andersson, Characterization of vanadia supported on amorphous AlPO4 and its properties for oxidative dehydrogenation of propane, Appl. Catal. A 112 (2) (1994) 187–208.
[39] L.S. Dake, D.R. Baer, D.M. Friedrich, Auger parameter measurements of phosphorus compounds for characterization of phosphazenes, J. Vac. Sci. Technol. A 7 (3) (1989) 1634–1638.
[40] J.F. Moulder, J. Chastain, Handbook of X-ray Photoelectron Spectroscopy: A Reference Book of Standard Spectra for Identification and Interpretation of XPS Data, Physical Electronics Division, Perkin-Elmer Corporation1992.
[41] https://srdata.nist.gov/xps/EngElmSrchQuery.aspx?EType=PE&CSOpt=Retri_ex_dat&Elm=P.
[42] R.J. Kirkpatrick, R.K. Brow, Nuclear magnetic resonance investigation of the structures of phosphate and phosphate-containing glasses: a review, Solid State Nucl. Magn. Reson. 5 (1) (1995) 9–21.
[43] S. Hunger, H. Cho, J.T. Sims, D.L. Sparks, Direct Speciation of Phosphorus in Alum-Amended Poultry Litter: Solid-State 31P NMR Investigation, Environ. Sci. Tech. 38 (2004) 674–681.
[44] E.C. de Oliveira Lima, J.M. Moita Neto, F.Y. Fujiwara, F. Galembeck, Aluminum Polyphosphate Thermoreversible Gels: A Study by31P and27Al NMR Spectroscopy, J. Colloid Interface Sci. 176 (1995) 388–396.
[45] H. Kwak Ja, J. Hu, D. Mei, C.-W. Yi, H. Kim Do, H.F. Peden Charles, F. Allard Lawrence, J. Szanyi, Coordinatively Unsaturated Al3+ Centers as Binding Sites for Active Catalyst Phases of Platinum on γ-Al2O3, Science 325 (2009) 1670–1673.
[46] K. Damodaran, J.W. Wiench, S.M. Cabral de Menezes, Y.L. Lam, J. Trebosc, J. P. Amoureux, M. Pruski, Modification of H-ZSM-5 zeolites with phosphorus. 2. Interaction between phosphorus and aluminum studied by solid-state NMR spectroscopy, Microporous Mesoporous Mater. 95 (2006) 296–305.
[47] G. Caeiro, P. Magnoux, J.M. Lopes, F.R. Ribeiro, S.M.C. Menezes, A.F. Costa, H. S. Cerqueira, Stabilization effect of phosphorus on steamed H-MFI zeolites, Appl. Catal. A 314 (2) (2006) 160–171.
[48] G. Lischke, R. Eckelt, H.G. Jerschkewitz, B. Parlitz, E. Schreier, W. Storek, B. Zibrowius, G. Öhlmann, Spectroscopic and physicochemical characterization of P-Modified H-ZSM-5, J. Catal. 132 (1991) 229–243.
[49] R. Baran, Y. Millot, T. Onfroy, J.-M. Krafft, S. Dzwigaj, Influence of the nitric acid treatment on Al removal, framework composition and acidity of BEA zeolite investigated by XRD, FTIR and NMR, Microporous Mesoporous Mater. 163 (2012) 122–130.
[50] T. Blasco, A. Corma, J. Martínez-Triguero, Hydrothermal stabilization of ZSM-5 catalytic-cracking additives by phosphorus addition, J. Catal. 237 (2006) 267–277.